
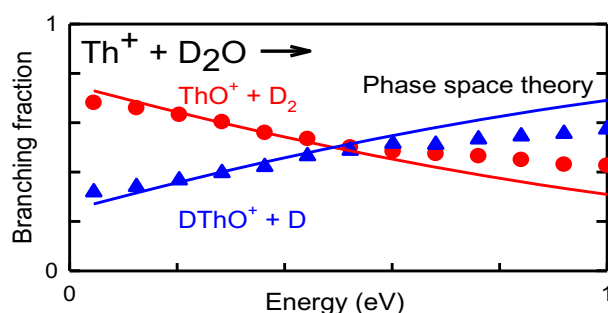


# Activation of Water by Thorium Cation: A Guided Ion Beam and Quantum Chemical Study

Richard M. Cox,<sup>1,2</sup> P. B. Armentrout<sup>1</sup> 

<sup>1</sup>Department of Chemistry, University of Utah, Salt Lake City, UT 84112-0850, USA

<sup>2</sup>Pacific Northwest National Laboratory, 902 Battelle Blvd, Richland, WA 99354, USA



**Abstract.** The reaction of atomic thorium cations with deuterated water as a function of kinetic energy from thermal to 10 eV was studied using guided ion beam tandem mass spectrometry. At thermal energies, both  $\text{ThO}^+ + \text{D}_2$  and  $\text{DThO}^+ + \text{D}$  are formed in barrierless exothermic processes and reproduce results in the literature obtained using ion cyclotron resonance mass spectrometry. As the energy is increased, the branching ratio between these two channels changes such

that the dominant product changes from  $\text{ThO}^+$  to  $\text{DThO}^+$  and back to  $\text{ThO}^+$ , until  $\text{ThD}^+ + \text{OD}$  is energetically available and is the dominant product channel. To help understand these experimental results, a variety of theoretical approaches were tried and used to establish a potential energy surface, which compares well with previous theoretical studies. Utilizing the theoretical results, the kinetic energy dependent branching ratio between the  $\text{ThO}^+ + \text{D}_2$  and  $\text{DThO}^+ + \text{D}$  channels was calculated using both RRKM and phase space theory (PST). The results indicate that consideration of angular momentum conservation (as in PST) and spin-orbit corrected energies are needed to reproduce experimental results quantitatively. The PST modeling also provides relative energies for the two competing transition states that lead to the primary products, for which theory provides reasonable agreement.

**Keywords:** Actinide chemistry, Bond activation, Gas-phase ion chemistry, Tandem mass spectrometry, Thermodynamics

Received: 11 January 2019/Revised: 15 February 2019/Accepted: 15 February 2019/Published Online: 16 April 2019

## Introduction

Actinide chemistry is of interest for multiple reasons, including its applicability to nuclear power generation where members of the actinide series are either used as a fuel or are a byproduct from the nuclear process. Although nuclear power remains a viable and efficient source of energy, the risk of a breach or other incident during use or storage of materials remains significant. Consequently, a thorough understanding of actinide reactivity is warranted to help identify, assess, and model potential

contamination dispersion in the event of a nuclear incident. The actinide-water reaction is of particular interest because water is a common coolant and neutron moderator in many reactor designs so that nuclear fuels and water are in close proximity.

Despite this interest, actinide chemistry remains difficult to study experimentally because of the extreme radioactivity of all members except Th and U, which are only mildly radioactive. Theoretical studies are a potentially promising alternative that mitigates any safety concerns regarding the handling of actinides in experimental studies. To validate such theoretical approaches, it is critical to have experimental work available for comparison. Several groups, including our own and that of Helmut Schwarz, have endeavored to establish accurate experimental benchmarks for gas-phase actinide compounds to which theoretical values can be directly and easily compared [1–26]. This experimental information includes bond lengths,

**Electronic supplementary material** The online version of this article (<https://doi.org/10.1007/s13361-019-02162-1>) contains supplementary material, which is available to authorized users.

Correspondence to: P. B. Armentrout; e-mail: armentrout@chem.utah.edu

energy levels, and thermodynamic values such as bond energies and ionization energies. Another potential experimental benchmark to which theory can be compared is the rates and branching ratios of chemical reactions.

One particular reaction for which experimental and theoretical results have already been compared is the activation of water by atomic thorium cations. This reaction has been studied previously in two Fourier-transform ion cyclotron resonance (FT-ICR) mass spectrometry experiments at thermal energies, first by Schwarz and coworkers [9] and later by Santos et al. [16]. In both studies, a branching ratio of 65%  $\text{ThO}^+ + \text{H}_2$  to 35%  $[\text{Th}_2\text{O}, \text{H}]^+ + \text{H}$  was observed. A subsequent potential energy surface (PES) presented by Mazzone et al. [27] indicates that the hydrido thorium oxide,  $\text{HThO}^+$ , is energetically preferred compared to the thorium hydroxide,  $\text{ThOH}^+$ , and that the  $\text{ThO}^+$  and  $\text{HThO}^+$  products share a common intermediate,  $\text{HThOH}^+$ . Furthermore, barriers relative to the shared intermediate for  $\text{ThO}^+$  and  $\text{HThO}^+$  for the rate-limiting steps of each reaction were determined to be 0.86–1.26 and 2.00–2.32 eV, respectively (2.83–3.94 and 1.78–2.80 eV below ground state reactants, respectively). In this study, no spin-orbit effects were considered, which could alter the conclusions as these corrections are typically large for  $\text{Th}^+$ . A second theoretical study by Zhou and Schlegel [28] essentially duplicates the PES presented by Mazzone et al. and also includes a theoretical determination of the  $\text{ThO}^+/\text{HThO}^+$  branching ratio by calculating the Rice–Ramsperger–Kassel–Marcus (RRKM) theory [29, 30] rate constant for each product channel restricted by their respective rate-limiting step. Despite the clear thermodynamic preference for the  $\text{ThO}^+ + \text{H}_2$  products, Zhou and Schlegel found that RRKM rate constants calculated using their derived PES predict that the  $\text{HThO}^+ + \text{H}$  channel should dominate, giving a 11:89  $\text{ThO}^+/\text{HThO}^+$  branching ratio in clear contradiction to the experimentally observed branching pattern. Their conclusion was that the energy available may be large enough that the reaction proceeded more rapidly than energy redistribution so that a statistical treatment was not valid. In contrast, a semi-empirical trajectory study presented in the same paper observed an  $\sim 80:20$   $\text{ThO}^+/\text{HThO}^+$  branching ratio in better agreement with the experimental results, but still not quantitative. Notably, Zhou and Schlegel indicate that a majority of their trajectories failed to dissociate to product in the simulation timeframe so that additional time was added to the simulation of several (16) trajectories to obtain the reported branching ratio for these simulations. Such an observation suggests that the intermediate common to the products is sufficiently long lived that statistical energy redistribution throughout the modes is likely. Here, spin-orbit effects were considered (using a zero-order regular approximation with spin-orbit, ZORA-SO, approach), but the  $\text{Th}^+ + \text{H}_2\text{O}$  asymptote was not included (meaning that the return to reactants was not considered). Rather the trajectories were started at the transition state for insertion of  $\text{Th}^+$  into the OH bond of water. This approximation should adversely affect the distribution of angular momentum available in the trajectories and also means the efficiency of the reaction is not correctly considered, potentially biasing the branching ratio results.

In recent studies of  $\text{Th}^+$  reactions [24–26], we have employed a first-order, semi-empirical spin-orbit energy correction that employs the experimentally determined  $\text{Th}^+ \zeta(6d)$  parameter and the experimental  $\text{Th}^+$  levels to correct molecular energies. For  $\text{ThH}^+$  and  $\text{ThO}^+$ , these estimated spin-orbit corrections were within 0.01 eV of theoretically calculated spin-orbit corrections [25, 26]. In our study of the activation of  $\text{CH}_4$  by  $\text{Th}^+$  [24], it was concluded that the inclusion of the spin-orbit parameter was essential to reproduce the energy of the experimentally observed barrier for C–H bond activation.

Here, we present absolute cross-sections as a function of reactant kinetic energy for the reaction of  $\text{Th}^+ + \text{D}_2\text{O}$  observed using guided ion beam tandem mass spectrometry (GIBMS). An analysis of these data allows the determination of the experimental energies of the rate-limiting steps relative to the reactants by modeling the kinetic energy dependences of the  $\text{ThO}^+ + \text{D}_2$  and  $\text{DThO}^+ + \text{D}$  reaction cross-sections using phase space theory (PST), which explicitly conserves angular momentum during the reactions. The kinetic energy dependence of the branching ratio (and related cross-sections) acts as a much more stringent test of the theoretical energies than the lone thermal energy branching ratio available in the literature. We also present quantum chemical calculations of the  $\text{Th}^+ + \text{H}_2\text{O}$  reaction coordinate using various levels of theory and basis sets. From these energies, we calculate the RRKM and PST  $\text{ThO}^+/\text{HThO}^+$  branching ratios at thermal energies before and after explicitly including spin-orbit energy corrections. For the present reaction of  $\text{Th}^+ + \text{H}_2\text{O}$ , the accuracy of the calculated energy of each respective rate-limiting transition state relative to each other and the reactants is shown to be critical to successfully reproducing the experimentally observed branching ratio. Both spin-orbit corrections and consideration of angular momentum conservation are required for quantitative agreement.

## Experimental and Theoretical Methods

### Instrument

The GIBMS used in these experiments has been described in detail previously [31]. Briefly, ions were created in a direct current discharge/flow tube source (DC/FT) [32] where a cathode holding the thorium powder sample was held at  $\sim 2.5$  kV. The resulting electric field ionized Ar in a 9:1 He/Ar mixture flowing over the electrode. Ar ions created in the discharge collided with the cathode, sputtering  $\text{Th}^+$  ions. The  $\text{Th}^+$  ions were swept along the flow tube by the He/Ar carrier gas mixture at a total pressure of 0.3–0.4 Torr where the  $\text{Th}^+$  is thermalized by  $\sim 10^5$  collisions with the carrier gas. Previous experiments [33–37] have indicated that the electronic state distribution of the metal ions produced by the DC/FT source can be characterized by a temperature between 300 and 1100 K. Conservatively, we estimate an internal energy of  $700 \pm 400$  K, such that 91.9% of ions are found in the ground level ( $^4\text{F}_{3/2}$ ,  $6d^27s$ ) with an average electronic energy ( $E_{\text{el}}$ ) of  $0.02 \pm 0.03$  eV. In the present and previous experiments with

thorium cations [24–26], no evidence of excited electronic states was observed.

After exiting the source, ions were focused through a magnetic momentum analyzer where the reactant  $^{232}\text{Th}^+$  ion beam was mass selected. These ions were decelerated to a well-defined kinetic energy and passed into a radio frequency (rf) octopole ion guide [38, 39] that constrained the ions radially. The octopole passes through a static pressure reaction cell that contained the neutral reaction partner  $\text{D}_2\text{O}$ . Prior to use, nitrogen was bubbled through the  $\text{D}_2\text{O}$  for  $\sim 20$  min in order to remove oxygen, and the  $\text{D}_2\text{O}$  was subsequently held under low vacuum for  $\sim 1$  h.  $\text{D}_2\text{O}$  was introduced into the reaction cell by mild heating of the liquid's container with a room temperature water bath. To ensure that the probability of multiple collisions between  $\text{Th}^+$  and the neutral gas were sufficiently small, the pressure in the reaction cell was maintained at typical pressures of 0.05–0.20 mTorr. Independent measurements at several pressures were performed to determine the reaction cross-section dependence on the neutral reactant pressures. Reaction cross-sections were calculated from product ion intensities relative to reactant ion intensities after correcting for background ion intensities measured when the neutral gas was no longer directed into the gas cell [40]. Cross-sections were extrapolated to rigorous single collision conditions (zero pressure conditions) using the determined cross-section dependence on reactant gas pressures. Uncertainties in the calculated absolute cross-sections are estimated to be  $\pm 20\%$ , with relative uncertainties of  $\pm 5\%$ .

Laboratory ion energies (lab) were converted to the center-of-mass frame (CM) using the relationship  $E = E_{\text{lab}} \times m / (m + M)$  where  $m$  and  $M$  are the masses of the reactant neutral and ion, respectively. At very low energies, the conversion includes a correction for the truncation of the ion kinetic energy distribution, as described previously [40]. Cross-sections are known to be broadened by the kinetic energy distribution of the reactant ions and the thermal (300 K) motion of the neutral reactant [41]. The absolute zero of energy and the full width at half-maximum (fwhm) of the ion beam were determined by using the octopole guide as a retarding potential analyzer, as described previously [40]. Typical fwhms of the ion kinetic energy distribution for these experiments were  $0.04 \pm 0.01$  eV (CM). Uncertainties in the absolute energy scale are  $\pm 0.008$  eV (CM). All energies reported below are in the CM frame.

## Data Analysis

**Phase Space Theory** Phase space theory (PST), originally developed by Light and Nikitin [42–44], is a statistical model for describing reactive collisions that assumes there is a strong interaction region from which the system decomposes statistically into all energetically possible reactant and product states. Here, we perform the PST calculation using modified versions of programs originally developed by Chesnavich and Bowers [45]. These calculations assumed that the potential interaction for the bimolecular reactants and products are ion-dipole and ion-induced dipole attractions, using the locked dipole cross-section [46–48] or trajectory collision model [49], and then

explicitly conserves both energy and angular momentum. The approach used here is described in greater detail in previous works [50].

**Modified Line-of-Centers Model** Endothermic reaction cross-sections were modeled using Eq. 1 [39, 51, 52],

$$\sigma(E) = \sigma_0 \sum g_i (E + E_{\text{el}} + E_i - E_0)^n / E \quad (1)$$

where  $\sigma_0$  is an energy-independent scaling factor,  $E$  is the relative kinetic energy of the reactants,  $E_{\text{el}}$  is the electronic energy of the reactant ion (as defined above),  $E_i$  is the internal energy of the neutral reactants having populations  $g_i$  ( $\sum g_i = 1$ ),  $n$  is an adjustable parameter that controls the shape of the cross-section, and  $E_0$  is the 0 K reaction threshold. Before comparison to the data, Eq. 1 was convoluted over the kinetic energy distributions of the reactants. The  $\sigma_0$ ,  $n$ , and  $E_0$  parameters were then optimized using a nonlinear least-squares method to best reproduce the experimental cross-section [40, 53]. Uncertainties in  $E_0$  were calculated from the threshold values from several independent data sets over an acceptable range of  $n$  values and were combined with the absolute uncertainties in the kinetic energy scale and electronic energies of reactant ions ( $E_{\text{el}} = 0.02 \pm 0.03$  eV). At high energies, cross-sections decline because enough energy is available for products to dissociate. To reproduce experimental cross-sections in this energy region, Eq. 1 is modified to include a statistical model of the dissociation probability [54], which is controlled by two adjustable parameters:  $p$ , which is similar to  $n$ , but can hold only integer values; and  $E_d$ , the energy at which product cross-sections begin to decline. The inclusion of the high-energy model in the present work does not significantly alter the threshold analyses of  $E_0$ .

In the limit that the threshold for the reaction  $\text{Th}^+ + \text{LR} \rightarrow \text{ThL}^+ + \text{R}$  corresponds to the thermodynamic onset for formation of the products, the  $E_0$  obtained from Eq. 1 can be used to determine the bond dissociation energy (BDE),  $D_0(\text{Th}^+-\text{L})$ , using Eq. 2.

$$D_0(\text{Th}^+-\text{L}) = D_0(\text{L}-\text{R}) - E_0 \quad (2)$$

This limit often holds for ion-molecule reactions because of the long-range attractive forces. Its validity can be tested by comparison with theoretical potential energy surfaces, as discussed further below.

## Theoretical Calculations

Quantum chemical calculations were performed using the Gaussian 09 suite of programs [55]. In most calculations, polarized correlation consistent core-valence quadruple- $\zeta$  (20s17p12d11f7g4h1i)/[9s9p8d8f7g4h1i] and triple- $\zeta$  (17s16p11d10f4g1h)/[8s8p7d6f4g1h] basis sets for Th [56] were used in combination with the Stuttgart–Cologne (MDF) small core (60 electron) relativistic effective core potential (ECP) [57]. For O and H atoms, polarized correlation consistent basis sets of the same quality were used, cc-pwCVXZ

( $X = T, Q$ ) [58]. Extrapolation to the complete basis set limit (CBS) for the cc-pwCVXZ ( $X = T, Q$ ) basis sets [56, 59] was performed using the Karton–Martin method [60], Eq. 3, for HF energies (where  $x = 3$  for T and  $x = 4$  for Q).

$$E_x = E_{\text{CBS}} + A(x + 1)e^{-6.57/x} \quad (3)$$

For CCSD(T)/cc-pwCVXZ calculations, Eq. 4 [61] is used to extrapolate the correlation energy.

$$E_x = E_{\text{CBS}} + B(x + 1/2)^{-4} \quad (4)$$

For correlation to previous results [24–26], calculations were also performed using the cc-pwCVQZ basis set for  $\text{Th}^+$  with an augmented aug-cc-pwCVQZ basis set for O and H as well as the Stuttgart–Dresden (SDD) basis set and a similar segmented Stuttgart–Dresden (Seg. SDD) basis set for  $\text{Th}^+$  [62, 63]. The latter two basis sets both employ a small core quasi-relativistic ECP (MWB) and are double- $\zeta$  and quadruple- $\zeta$  in quality, respectively. These basis sets were used with a Pople 6–311++G(3df,3p) basis set [64] for O and H.

For calculations utilizing the MWB ECP, structures were optimized using B3LYP in combination with the SDD basis set for  $\text{Th}^+$  and the 6–311++G(3df,3p) basis set for O and H, B3LYP/SDD/6–311++G(3df,3p). For calculations utilizing the MDF ECP, structures were optimized using PBE0/cc-pVQZ/cc-pVTZ. This latter approach was successfully used in the previous theoretical treatment of the  $\text{Th}^+ + \text{CH}_4$  reaction [24]. Single point energies of the optimized structures were calculated using the B3LYP [65, 66], B3PW91 [67], BH and HLYP (BHLYP) [66], M06 [68], and PBE0 [69] functionals. Additional single point calculations were performed using a coupled cluster method that includes single, double, and perturbative triple excitations, CCSD(T) [70–72]. For calculation of the correlation energy, the  $\text{Th}^+$   $5s$  and  $5p$  electrons and O  $1s$  electrons were frozen. All reported energies are zero-point energy corrected using the frequencies from the respective optimized structure after scaling the frequencies by 0.989 [73, 74].

### Spin-Orbit Corrections

Additionally, all calculations were corrected for spin-orbit effects using a semi-empirical model that has been described in detail previously [24, 75, 76]. Briefly, the theoretical calculations described above yield energies that are the average over all spin-orbit states. For  $\text{Th}^+$ , the  $J = 3/2$  ground level is a mixture of the  $^4\text{F}_{3/2}$  ( $6d^27s$ ) and  $^2\text{D}_{3/2}$  ( $6d7s^2$ ) levels [77, 78], with the  $^4\text{F}_{3/2}$  comprising the primary contribution (see Ref. [24] and its supplementary material for more detail). A nuance of the  $\text{Th}^+$  system is that although the experimental ground level is best described as  $^4\text{F}_{3/2}$ , the ground state is  $^2\text{D}$  ( $6d7s^2$ ), 0.06 eV lower in energy than the  $^4\text{F}$  state ( $6d^27s$ ) when averaged over all spin-orbit levels. The  $^4\text{F}_{3/2}$  ground level lies 0.46 eV lower in energy than the average  $^4\text{F}$  state and the  $^2\text{D}_{3/2}$  level lies 0.18 eV lower in energy than the average  $^2\text{D}$  state. For the  $\text{Th}^+ + \text{H}_2\text{O}$  reactants, spin-orbit effects were

included by correcting the calculated energies by the empirical difference between the  $^2\text{D}$  ground state and the  $^4\text{F}_{3/2}$  ground level,  $-0.40$  eV. With the exception of the first intermediate along the potential energy surface, discussed below, all other species along the potential energy surface are A states or otherwise singly degenerate so that no explicit first-order spin-orbit corrections according to this model are needed. The net effect is that all calculated energies shift up by 0.40 eV relative to the experimental  $\text{Th}^+ (^4\text{F}_{3/2}) + \text{H}_2\text{O}$  reactant asymptote compared to the  $\text{Th}^+ (^2\text{D}) + \text{H}_2\text{O}$  asymptote.

The first intermediate,  $\text{Th}^+(\text{H}_2\text{O})$ , is best characterized as a non-covalent interaction between the charged  $\text{Th}^+$  and polar  $\text{H}_2\text{O}$ . Previously [24], for the comparable  $\text{Th}^+(\text{CH}_4)$  intermediate, we hypothesized that because the interaction between  $\text{Th}^+$  and the ligand is minimal, the spin-orbit splitting of this intermediate could be estimated as similar to that of the unperturbed metal, an approximation that led to consistency with the experimental measurement of  $\text{D}_0(\text{Th}^+ - \text{CH}_4)$ . Therefore, this same approximation is used here for  $\text{Th}^+(\text{H}_2\text{O})$ . Overall, this approach may be simplistic because a much stronger interaction between  $\text{Th}^+(\text{H}_2\text{O})$  is anticipated compared to  $\text{Th}^+(\text{CH}_4)$ ; however, a more exact treatment of the spin-orbit splitting of this intermediate is beyond the scope of this work and furthermore would not change any conclusions made from the results reported therein.

### Theoretical Branching Ratios

Theoretical rate constants were calculated using RRKM theory [29, 30] and PST [42–45, 51]. Frequencies and rotational constants used in these calculations were taken from the optimized structures of the appropriate transition states and their preceding intermediate after scaling the vibrational frequencies by 0.989. The number of states available in the transition states and the density of states in the intermediate were calculated using the Beyer–Swinehart–Stein–Rabinovitch algorithm [79–81].

## Results

### Experimental Results

Kinetic energy dependent cross-sections for the reaction of  $\text{Th}^+$  with  $\text{D}_2\text{O}$  are presented in Fig. 1. Products are formed according to the following reactions:



Clearly, products formed at low energy containing two oxygen atoms must be formed in sequential reactions of the primary  $\text{ThO}^+$  and  $[\text{Th}, \text{O}, \text{D}]^+$  products. This is confirmed by the fact that

the cross-sections for  $\text{ThO}_2^+$  and  $\text{ThO}_2\text{D}^+$  products increase linearly with  $\text{D}_2\text{O}$  pressure. These sequential reactions are easily eliminated by extrapolating the cross sections to zero-pressure conditions, which affects only the lowest energy points shown in Fig. 1 for  $\text{ThO}^+$  and  $[\text{Th},\text{O},\text{D}]^+$ . The remaining description here refers to such zero-pressure extrapolated results.

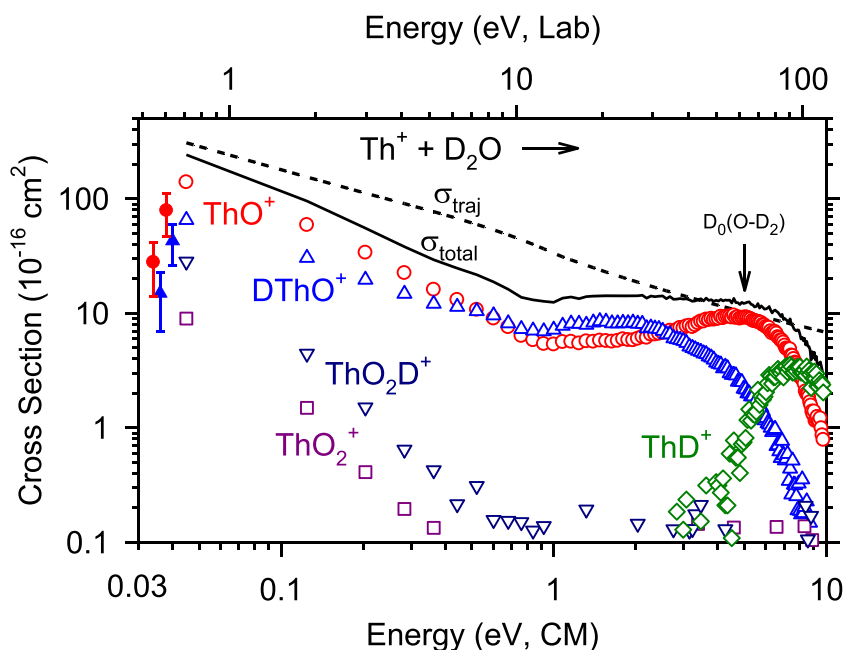
Compared with the collision cross-section,  $\sigma_{\text{traj}}$ , calculated according to the trajectory model of Su and Chesnavich [49], the total reaction (i.e., the sum of reactions 5–9) proceeds with  $\sigma_{\text{total}}/\sigma_{\text{traj}} = 0.68 \pm 0.14$  efficiency at 0.05 eV, equivalent to thermal energies. This value is similar to the reaction efficiency observed by Cornehl et al. [9] in FT-ICR experiments ( $0.57 \pm 0.23$ ), which are somewhat higher than those of Santos et al. [16] ( $0.20 \pm 0.10$ ). Neither of these studies reported absolute rates, but only efficiencies relative to a collision limit calculated using average dipole orientation (ADO) theory [48], which we calculate as equivalent to having a 300 K (0.039 eV) cross-section of  $214 \times 10^{-16} \text{ cm}^2$ , whereas  $\sigma_{\text{traj}}(0.039 \text{ eV}) = 340 \times 10^{-16} \text{ cm}^2$ . When this ADO cross-section is combined with their reaction efficiencies, the effective cross-sections measured in these studies are shown in Fig. 1. The efficiency of the total reaction declines with increasing kinetic energy reaching a minimum of  $0.26 \pm 0.05$  at 0.76 eV. This result could explain the differences in the previous FT-ICR efficiencies if those of Santos et al. were at elevated energies. Different distributions of electronic levels of the  $\text{Th}^+$  reactant might also explain such differences. It is clear from Fig. 1 that reactions 5 and 6 are dominant at all but the highest energies with a 68:32  $\text{ThO}^+/\text{DThO}^+$  product branching ratio at 0.05 eV, nearly identical to the branching ratios observed at thermal energies in the FT-ICR experiments, 65:35 [9, 16].

Above thermal energies, the  $\text{ThO}^+$  and  $[\text{Th},\text{O},\text{D}]^+$  cross-sections behave differently with energy such that the branching ratio shifts to increasingly favor reaction 6 as energy increases, Fig. 2. The cross-section for formation of  $\text{ThO}^+$  in reaction 5 steadily declines until it reaches  $\sim 1 \text{ eV}$  where it levels out near  $6 \text{ \AA}^2$ . Similarly, the cross-section for formation of  $[\text{Th},\text{O},\text{D}]^+$  in reaction 6 declines with increasing energy until  $\sim 0.9 \text{ eV}$  before increasing slightly and leveling out at  $\sim 8 \text{ \AA}^2$ . The two cross-sections cross near 0.6 eV and the branching ratio nears 40:60  $\text{ThO}^+/\text{DThO}^+$  from about 1–1.5 eV. Also apparent is an endothermic feature in the  $\text{ThO}^+$  cross-section that begins to rise between 1 and 2 eV. The onset of this feature corresponds to the decline in intensity of the  $[\text{Th},\text{O},\text{D}]^+$  cross-section, suggesting that this feature could result from decomposition of  $[\text{Th},\text{O},\text{D}]^+$  into  $\text{ThO}^+ + \text{D}$  according to the overall reaction 10.

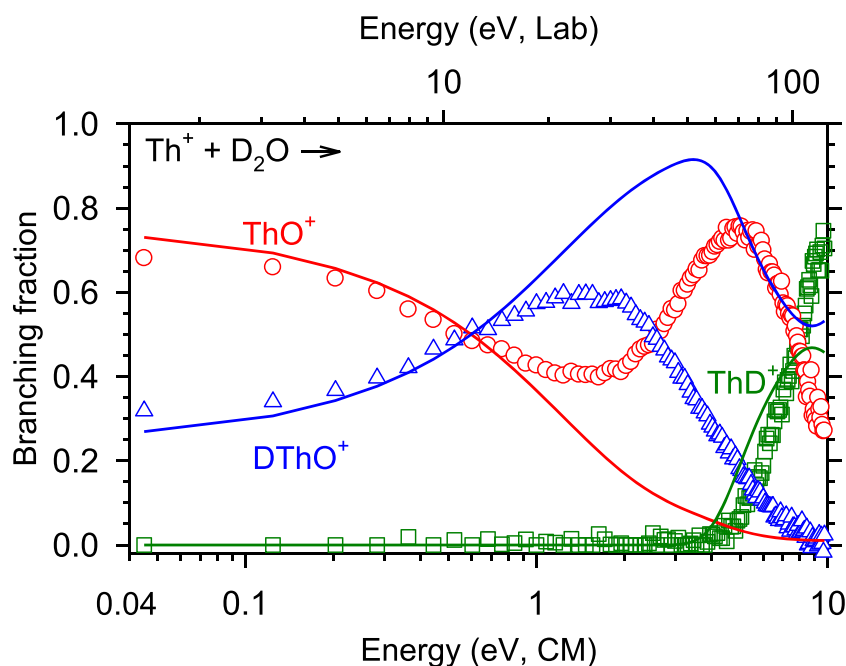


This hypothesis is supported by the thermochemistry discussed below. The  $\text{ThO}^+$  cross-section begins to decline sharply above about 5 eV, consistent with the threshold for  $\text{Th}^+ + \text{O} + \text{D}_2$  formation at  $D_0(\text{O}-\text{D}_2) = 5.110 \pm 0.001 \text{ eV}$  [82].

Reaction 7 is endothermic with an apparent threshold near 3 eV. Although this product could begin to dissociate beginning at  $D_0(\text{D}-\text{OD}) = 5.212 \pm 0.002 \text{ eV}$  [82], the fact that its cross-section does not peak until about 7 eV indicates that the OD product of reaction 7 carries away considerable energy. The rise in the  $\text{ThD}^+$  cross-section occurs at an energy where the  $[\text{Th},\text{O},\text{D}]^+$  cross-section for reaction 6 declines; however,

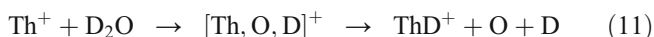


**Figure 1.** Product cross-sections for the reaction of  $\text{Th}^+$  with  $\text{D}_2\text{O}$  at a pressure of 0.1 mTorr as a function of kinetic energy in the laboratory (upper x-axis) and center-of-mass (lower x-axis) frames. The total cross-section is shown by the black line and the Su-Chesnavich variational trajectory cross-section is shown by the black dashed line. Solid symbols show the results of Cornehl et al. [9] (to the right) and Santos et al. [16] (to the left) converted to effective cross-sections at 0.039 eV



**Figure 2.** Experimental branching ratios of reactions 5–7 as a function of kinetic energy in the laboratory (upper x-axis) and center-of-mass (lower x-axis) frames. The lines show the PST predicted results using optimized energies of  ${}^2\text{TS2/3}$  and  ${}^2\text{TS2/4}$  as discussed in the text

decomposition of  $[\text{Th},\text{O},\text{D}]^+$  according to reaction 11 cannot occur until higher energies,  $7.14 \pm 0.05$  eV.



Therefore, any coupling between the  $\text{ThD}^+ + \text{OD}$  and  $[\text{Th},\text{O},\text{D}]^+$  channels would be the result of the two products sharing a common intermediate.

### Thermochemical and Theoretical Results

**$\text{ThO}^+$**  The energy dependence of reaction 5 below 1 eV, Fig. 1, is consistent with a barrierless, exothermic reaction indicating that  $D_0(\text{Th}^+-\text{O}) \geq D_0(\text{O}-\text{D}_2) = 5.110$  eV. This result is in good agreement with recent GIBMS work [26] that determined  $D_0(\text{Th}^+-\text{O}) = 8.57 \pm 0.14$  eV, as well as previous estimates of  $D_0(\text{Th}^+-\text{O}) = 8.74 \pm 0.26$  eV [21] and  $8.70 \pm 0.10$  eV [83] derived from  $D_0(\text{ThO})$ ,  $\text{IE}(\text{ThO})$ , and  $\text{IE}(\text{Th})$ .

At higher energies, a second feature with an energy dependence consistent with an endothermic reaction is observed, suggested to be reaction 10 above. The enthalpy of this reaction can be calculated according to Eq. 12.

$$\Delta_r H(10) = D_0(\text{O}-\text{D}_2) + D_0(\text{D}-\text{D}) - D_0(\text{Th}^+-\text{O}) \quad (12)$$

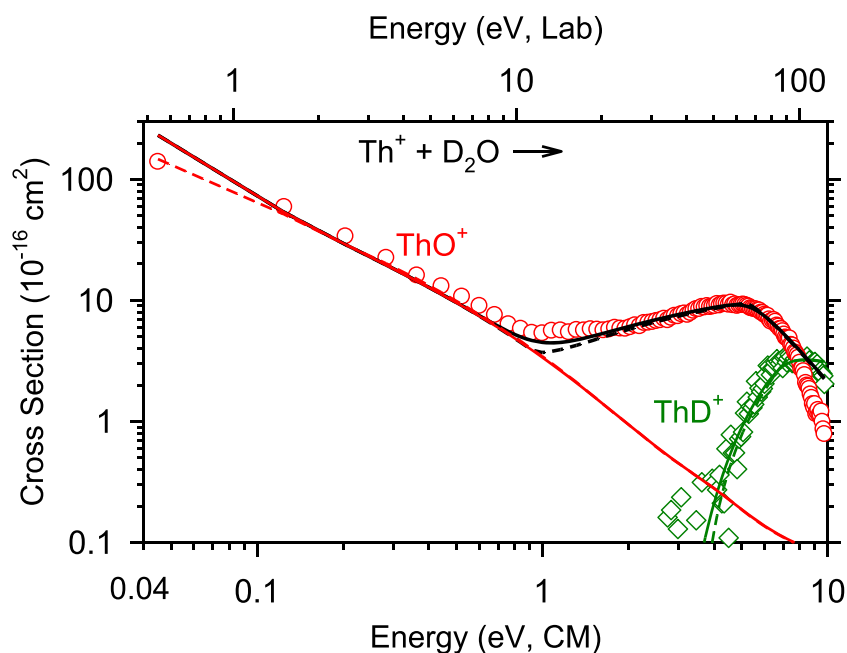
Given  $D_0(\text{O}-\text{D}_2) = 5.110 \pm 0.001$  eV and  $D_0(\text{D}-\text{D}) = 4.55622 \pm 0.00001$  eV [84],  $D_0(\text{Th}^+-\text{O}) = 8.57 \pm 0.14$  eV [26] indicates the threshold for this reaction should occur at  $E_0 = 1.10 \pm 0.14$  eV consistent with the apparent threshold. This feature can be modeled using the modified line-of-centers model (LOC), Eq. 1, after accounting for the exothermic pathway using

a PST model, as described further below. This LOC model is shown in Fig. 3 with parameters listed in Table 1, and results in a threshold of  $E_0 = 0.94 \pm 0.30$  eV, which has a large uncertainty because of the complications of accounting for the exothermic feature in the  $\text{ThO}^+$  cross-section. The threshold obtained is in reasonable agreement with that expected from the literature thermochemistry.

A full theoretical exploration of the  $\text{ThO}^+$  species can be found elsewhere [26]. Briefly,  $\text{ThO}^+$  has a  ${}^2\Sigma^+$  ground state with a triple bond and the unpaired electron located in a molecular orbital largely composed of the Th 7s-orbital. Shifting the unpaired electron to a Th 6d-orbital leads to the lowest energy excited state, 0.58 eV higher in energy [18].

**$[\text{Th},\text{O},\text{D}]^+$**  The energy dependence of the  $[\text{Th},\text{O},\text{D}]^+$  cross-section at low energies shows that reaction 6 is also a barrierless, exothermic reaction, which means that  $D_0(\text{Th}^+-\text{OD}) \geq D_0(\text{D}-\text{OD}) = 5.212 \pm 0.002$  eV [82] (although this bond energy does not necessarily imply that the  $[\text{Th},\text{O},\text{D}]^+$  species is a hydroxide). The same observation made in previous reports for reaction with  $\text{H}_2\text{O}$  by Cornehl et al. [9] and Santos et al. [16] led them to report that  $D_0(\text{Th}^+-\text{OH}) \geq 5.10 \pm 0.01$  eV =  $D_0(\text{H}-\text{OH})$  [84]. The  $[\text{Th},\text{O},\text{D}]^+$  cross-section increases slightly starting near 1 eV. Identification of this feature in the cross-section requires additional information from theory and is discussed below.

Theoretical calculations indicate that the lowest energy structure of  $[\text{Th},\text{O},\text{H}]^+$  is a hydrido thorium oxide,  $\text{HThO}^+$ , with a  ${}^1\text{A}'$  ground state rather than the  $\text{ThOH}^+$  hydroxide. (Note that we will refer to  $[\text{Th},\text{O},\text{H}]^+$  as  $\text{HThO}^+$  for the remainder of



**Figure 3.** Model line-of-centers (LOC) cross-sections of endothermic features convoluted over the distributions of internal and translational reactant energies (solid lines) and in the absence of these distributions (dashed lines). The PST model for  $\text{ThO}^+$  is shown by the solid red line

the manuscript.) A  $^1\Sigma^+$  thorium hydroxide is found 0.3–1.3 eV higher in energy and a  $^3\Delta$  state of  $\text{ThOH}^+$  is found 0.7–1.4 eV above the  $\text{HThO}^+$  ground state. These and additional structures of  $[\text{Th},\text{O},\text{H}]^+$  located theoretically are listed in Tables S1 and S2. These results are consistent with the structures calculated by Mazzone et al. [27] and Zhou and Schlegel [28], who also found a  $\text{HThO}^+$  ( $^1A'$ ) ground state at various levels of theory using SDD/6–311++G(d,p) basis sets. Additionally, Zhou and Schlegel report a triplet  $\text{ThOH}^+$  (specific state not provided) lying 1.1 eV higher in energy than the  $^1A'$  ground state using PW91/SDD/6–311++G(d,p). Theoretical BDEs indicate that  $D_0(\text{Th}^+-\text{OH}) = 5.5\text{--}7.2$  eV (Table S3) indicating that reaction 6 is exothermic by 0.3–2.0 eV, consistent with observation.

*ThD<sup>+</sup>* Given  $D_0(\text{Th}^+-\text{D}) = 2.48 \pm 0.07$  eV determined in a previous GIBMS experiment of the reactions of  $\text{Th}^+ + \text{H}_2$  and  $\text{D}_2$  [25] and  $D_0(\text{DO}-\text{D}) = 5.212 \pm 0.002$  eV [82], reaction 7 should be endothermic by  $2.73 \pm 0.07$  eV, roughly consistent with observation, Fig. 1. As shown in Fig. 3, the cross-section for reaction 7 was modeled using Eq. 1, with parameters in Table 1. The threshold obtained,  $E_0 = 3.40 \pm 0.31$  eV, is somewhat above that predicted using the literature thermochemistry. The discrepancy is likely caused by competition of reaction 7 with the thermodynamically more favorable reactions 5 and 6,

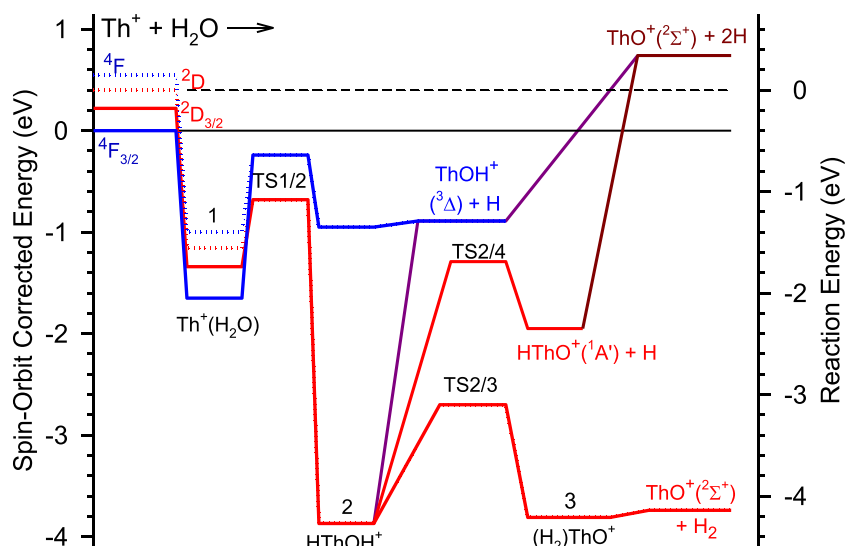
whereas the reaction with  $\text{D}_2$  has no competing channels. A similar shift in thermodynamic threshold was observed in the reaction of  $\text{Th}^+ + \text{CH}_4$  forming  $\text{ThH}^+ + \text{CH}_3$  where a shift of  $0.21 \pm 0.21$  eV was observed compared to the threshold expected on the basis of the reactions of  $\text{Th}^+ + \text{H}_2$  and  $\text{D}_2$ . This shift was subsequently verified by a PST modeling of the competing products in the  $\text{Th}^+ + \text{CH}_4$  reaction, formation of  $\text{ThCH}_2^+$ ,  $\text{ThH}^+$ , and  $\text{ThCH}_3^+$  [24]. This possibility is discussed further in the section below where the competing reactions 5–7 are modeled using PST.

### Potential Energy Surfaces

The potential energy surface (PES) calculated using CCSD(T)/CBS//PBE0/cc-pVQZ/cc-pVTZ for the reaction of  $\text{Th}^+ + \text{H}_2\text{O}$  is presented in Fig. 4, with the related structures presented in Fig. 5. Energies for all intermediates and transition states at this and additional levels of theory are tabulated in Table 2. After correcting for spin-orbit energy as described above, reported energies in Table 2 are relative to  $\text{Th}^+ (^4F_{3/2}, 6d^2 7s) + \text{H}_2\text{O}$ . (Uncorrected values are also listed in parentheses relative to  $\text{Th}^+ (^2D, 6d 7s^2) + \text{H}_2\text{O}$  for reference.) Energies calculated using several levels of theory and additional basis sets are listed in Table S4 in the Supplementary Material. Before correcting

**Table 1.** Fitting parameters from Eq. 1 for the indicated reaction cross-section

Reaction	$n$	$\sigma_0$	$E_0$ (eV)	$D_0(\text{Th}^+-\text{L})$ (eV)
$\text{Th}^+ + \text{D}_2\text{O} \rightarrow \text{ThO}^+ + 2 \text{D}$	$1.2 \pm 0.2$	$9.0 \pm 2.6$	$0.94 \pm 0.30$	$8.73 \pm 0.30$
$\text{Th}^+ + \text{D}_2\text{O} \rightarrow \text{ThD}^+ + \text{OD}$	$2.1 \pm 0.4$	$1.9 \pm 1.6$	$3.40 \pm 0.31$	$\geq 1.80 \pm 0.31$

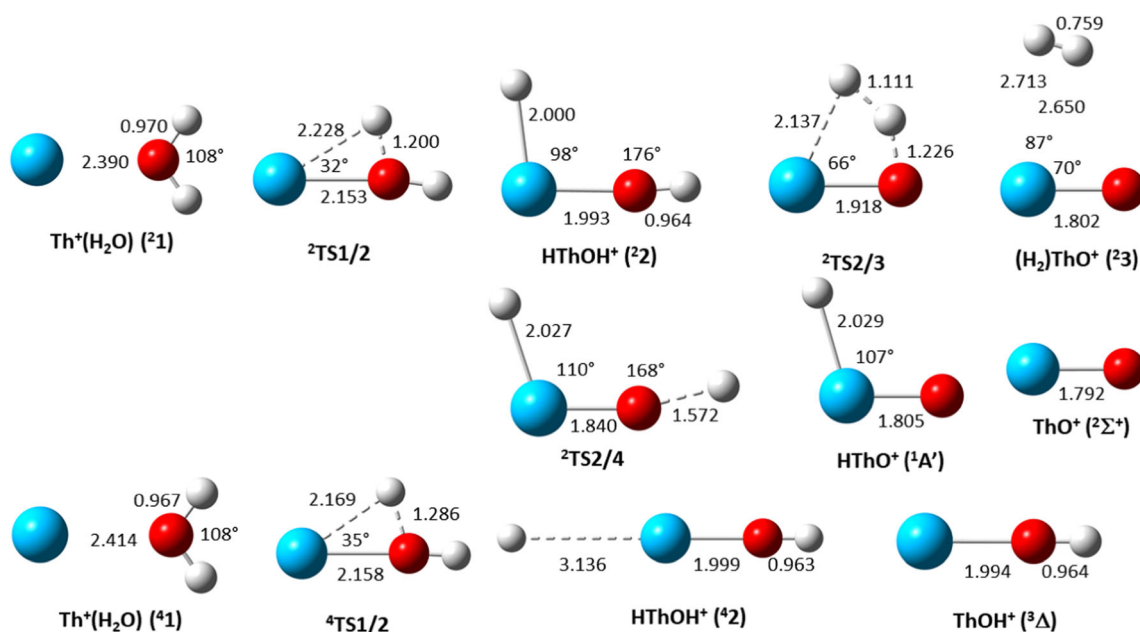


**Figure 4.** Potential energy surfaces for the two major products of the  $\text{Th}^+ + \text{H}_2\text{O}$  reaction. Single point energies calculated using CCSD(T)/CBS from PBE0/cc-pVQZ/cc-pVTZ optimized structures. Quartet spin surface in blue and doublet spin surface in red. Dotted lines represent the surfaces uncorrected for spin-orbit interactions (right-hand axis) whereas solid lines denote the spin-orbit corrected surface (left-hand axis)

for spin-orbit energy, the energies for all intermediates and transition states are similar to those reported previously by Mazzone et al. [27] and Zhou and Schlegel [28]. Without the spin-orbit correction, the doublet surface lies below the quartet surface throughout the entire reaction, whereas the introduction of the semi-empirical spin-orbit correction shifts the starting asymptote to the quartet surface suggesting a crossing between the doublet and quartet surfaces, a feature not suggested previously. However, the mixed state nature of the  $\text{Th}^+$   $J=3/2$  ground level ( $^4\text{F}_{3/2}$ ,  $^2\text{D}_{3/2}$ ) indicates that this crossing may be an artifact introduced by the need to designate a spin state in the

computations, as we have argued previously for a similar crossing in the  $\text{Th}^+ + \text{CH}_4$  PESs [24]. In reality, spin is likely a poor quantum number to describe ground level  $\text{Th}^+$  and its weakly bound adducts, and both doublet and quartet spin surfaces can evolve from the  $J=3/2$  ground level adduct.

*Doublet Surface* The first intermediate on the doublet surface,  $\text{Th}^+(\text{H}_2\text{O})$   $^2\mathbf{1}$ , has a  $^2\text{B}_2$  ground electronic state ( $^2\text{A}_2$  for M06) and lies 1.34 eV below the  $\text{Th}^+$  ( $^4\text{F}_{3/2}$ ,  $6d^27s$ ) +  $\text{H}_2\text{O}$  asymptote. The  $\angle\text{HOH}$  and  $r(\text{O-H})$  of  $^2\mathbf{1}$ , Fig. 5, are largely



**Figure 5.** Structures of intermediates and transition states along the  $\text{Th}^+ + \text{H}_2\text{O}$  potential energy surfaces shown in Fig. 4 as optimized at the PBE0/cc-pVQZ/cc-pVTZ level of theory. Select bond lengths (Å) and bond angles (°) are also provided



**Table 2.** Single point energies (eV) relative to  $\text{Th}^+ + \text{H}_2\text{O}$  reactants<sup>a</sup>

	CCSD(T) <sup>b</sup>	B3LYP	B3PW91	BHLYP	M06	PBE0
$\text{Th}^+ (^4\text{F}_{3/2}) + \text{H}_2\text{O}$	0.00 (0.15)	0.00	0.00	0.00	0.00	0.00
$\text{Th}^+ (^2\text{D}_{3/2}) + \text{H}_2\text{O}$	0.22 (0.00)	0.22	0.22	0.22	0.22	0.22
<b>21</b> ( <sup>2</sup> B <sub>2</sub> )	-1.34 (-1.56)	-1.41	-1.42	-1.27	-1.70	-1.47
<b>41</b> ( <sup>4</sup> B <sub>2</sub> )	-1.55 (-1.40)	-1.59	-1.60	-1.51	-1.80	-1.66
<b>2TS1/2</b> ( <sup>2</sup> A')	-0.68 (-1.08)	-0.89	-1.58	-0.46	-1.06	-0.91
<b>4TS1/2</b> ( <sup>4</sup> A'')	-0.24 (-0.64)	-0.44	-1.38	-0.11	-0.10	-0.70
<b>22</b> ( <sup>2</sup> A')	-3.87 (-4.27)	-3.98	-4.06	-3.75	-3.84	-4.07
<b>42</b> ( <sup>4</sup> A'')	-0.95 (-1.35)	-1.05	-1.22	-0.85	-2.53	-1.28
<b>2TS2/3</b> ( <sup>2</sup> A')	-2.70 (-3.10)	-2.78	-2.97	-2.26	-2.67	-2.97
<b>23</b> ( <sup>2</sup> A')	-3.81 (-4.21)	-3.83	-3.93	-3.39	-3.90	-3.90
<b>2TS2/4</b> ( <sup>2</sup> A')	-1.29 (-1.69)	-1.59	-1.68	-0.96	-1.52	-1.65
$\text{ThO}^+ (^2\Sigma^+) + \text{H}_2 (^1\Sigma_g^+)$	-3.74 (-4.14)	-3.80	-3.85	-3.35	-3.78	-3.77
$\text{HThO}^+ (^1\text{A}') + \text{H} (^2\text{S}_{1/2})$	-1.95 (-2.35)	-1.97	-2.18	-1.56	-2.20	-2.18
$\text{ThOH}^+ (^3\Delta_1) + \text{H} (^2\text{S}_{1/2})$	-0.89 (-1.29)	-1.00	-1.18	-0.81	-0.80	-1.22
$\text{ThH}^+ (^2\Delta_1) + \text{OH} (^2\Pi)$	2.36 (2.14)	2.07	2.04	2.00	2.41	2.06

<sup>a</sup>Single point energies at indicated level of theory using the complete basis set extrapolation from Method/cc-pwCVXZ/cc-pwCVXZ//PBE0/cc-pVQZ/cc-pVTZ calculations where X = T, Q. Spin-orbit corrections applied as indicated in the text. See also Fig. 4 for potential energy surface and Fig. 5 for structures

<sup>b</sup>Values in parentheses do not include spin-orbit corrections

unperturbed from those of free water,  $\angle\text{HOH} = 104^\circ$  and  $r(\text{O}-\text{H}) = 0.96 \text{ \AA}$ , which suggests that **21** is an association complex between  $\text{Th}^+$  and  $\text{H}_2\text{O}$ . From **21**, OH bond activation occurs through **2TS1/2** (<sup>2</sup>A'). One O–H bond elongates to  $r(\text{O}-\text{H}) = 1.20 \text{ \AA}$  and rotates from  $\angle\text{ThOH} = 126^\circ$  in **21** to  $78^\circ$  while the  $r(\text{Th}^+-\text{O})$  bond length shortens to  $2.15 \text{ \AA}$ . This process forms **22**, a hydrido thorium hydroxide cation, which is the global minimum lying  $3.87 \text{ eV}$  below the reactant asymptote. It has a <sup>2</sup>A' ground state with  $r(\text{Th}^+-\text{H})$  and  $r(\text{Th}^+-\text{O})$ , Fig. 5, being nearly identical to the  $\text{Th}^+-\text{H}$  bond length in the diatomic  $\text{ThH}^+$  (<sup>3</sup>Δ) ground state calculated previously,  $r(\text{Th}^+-\text{H}) = 2.00 \text{ \AA}$  [25], and the  $\text{ThOH}^+$  (<sup>3</sup>Δ) bond length calculated here,  $r(\text{Th}^+-\text{OH}) = 1.99 \text{ \AA}$ . These comparisons indicate that there are covalent bonds between the metal center and both ligands in  $\text{HThO}^+$  (<sup>2</sup>A').

**22** is also a common intermediate between all three primary reaction channels, reactions 5–7. **22** is connected to the lowest energy products,  $\text{ThO}^+ + \text{H}_2$ , through **2TS2/3** (<sup>2</sup>A'). In **2TS2/3**, both hydrogens rotate toward each other forming a four-centered ring structure, Fig. 5. **2TS2/3** lies  $1.17 \text{ eV}$  above **22** and leads to **23**,  $(\text{H}_2)\text{ThO}^+$ . In **23**,  $r(\text{Th}^+-\text{O})$  shortens to  $1.80 \text{ \AA}$ , similar to  $r(\text{Th}^+-\text{O}) = 1.79 \text{ \AA}$  in ground state  $\text{ThO}^+$  (<sup>2</sup>Σ<sup>+</sup>), with  $r(\text{H}-\text{H}) = 0.76 \text{ \AA}$ , similar to  $r(\text{H}-\text{H}) = 0.75 \text{ \AA}$  in  $\text{H}_2$  (<sup>1</sup>Σ<sub>g</sub><sup>+</sup>). Thus, **23** can be understood as a weakly bound association complex between  $\text{ThO}^+$  (<sup>2</sup>Σ<sup>+</sup>) and  $\text{H}_2$ . **23** lies  $3.81 \text{ eV}$  below the reactant asymptote and readily dissociates to the  $\text{ThO}^+$  (<sup>2</sup>Σ<sup>+</sup>) +  $\text{H}_2$  (<sup>1</sup>Σ<sub>g</sub><sup>+</sup>) product asymptote, only  $0.07 \text{ eV}$  higher in energy. Given  $D_0(\text{O}-\text{H}_2) = 5.01 \text{ eV}$  at CCSD(T)/CBS (compared to the experimental BDE,  $5.0348 \pm 0.0003 \text{ eV}$  [84]), the  $\text{ThO}^+$  BDE is predicted to be  $D_0(\text{Th}^+-\text{O}) = 8.75 \text{ eV}$ , in reasonable agreement with the experimental value of  $8.57 \pm 0.14 \text{ eV}$  [26].

Alternatively, the reaction can proceed from **22** through **2TS2/4**. In **2TS2/4**,  $\angle\text{HThO}$  opens to  $110^\circ$  from  $98^\circ$  in **22** and  $r(\text{Th}^+-\text{O})$  contracts to  $1.84 \text{ \AA}$  while  $r(\text{O}-\text{H})$  increases from  $0.96 \text{ \AA}$  in **22** to  $1.57 \text{ \AA}$ . The transition state, **2TS2/4**, lies  $2.58 \text{ eV}$  above the global minimum ( $1.41 \text{ eV}$  higher in energy than **2TS2/3**) and leads directly to the  $\text{HThO}^+$  (<sup>1</sup>A') +  $\text{H}$  (<sup>2</sup>S) products that lie  $1.95 \text{ eV}$  below the reactants ( $1.92 \text{ eV}$  above

the global minimum). Given  $D_0(\text{HO}-\text{H}) = 5.08 \text{ eV}$  for CCSD(T)/CBS (compared to the experimental BDE,  $5.1014 \pm 0.0004 \text{ eV}$  [84]), dissociation of  $\text{HThO}^+$  to  $\text{Th}^+ + \text{OH}$  is predicted to require  $D_0(\text{Th}^+-\text{OH}) = 6.96 \text{ eV}$ . Intermediate **22** can also dissociate by breaking the  $\text{H}-\text{ThOH}^+$  bond, forming  $\text{ThOH}^+$  (<sup>3</sup>Δ) +  $\text{H}$  (<sup>2</sup>S), calculated to lie  $0.40 \text{ eV}$  above **2TS2/4**. Finally, at higher energies, **22** can dissociate directly to  $\text{ThH}^+$  (<sup>3</sup>Δ<sub>1</sub>) +  $\text{OH}$  (<sup>2</sup>Π), which is calculated to lie  $2.36 \text{ eV}$  above the reactants, in reasonable agreement with the experimental asymptote of  $2.65 \pm 0.07 \text{ eV}$  (given  $D_0(\text{Th}^+-\text{D}) = 2.48 \pm 0.07 \text{ eV}$  [25]).

**Quartet Surface** Along the quartet spin reaction surface, the first intermediate, **41**, has a <sup>4</sup>B<sub>2</sub> ground state that lies  $0.21 \text{ eV}$  lower in energy than **21**. <sup>4</sup>A<sub>2</sub> and <sup>4</sup>B<sub>1</sub> states were also found within  $0.5 \text{ eV}$  of **21** for all methods except M06, as listed in Table S4 in the Supplementary Material. The reaction along this surface evolves through **4TS1/2** to form **42**. **4TS1/2** (<sup>4</sup>A'') lies  $0.44 \text{ eV}$  higher in energy than **2TS1/2**. Geometrical parameters for **4TS1/2** are similar to those found for **2TS1/2**, Fig. 5. **42** (<sup>4</sup>A'') lies  $2.92 \text{ eV}$  higher in energy than **22** (<sup>2</sup>A'). Unlike **22** where  $r(\text{Th}-\text{H}) = 2.00 \text{ \AA}$ ,  $r(\text{Th}-\text{H})$  in **42** is  $3.14 \text{ \AA}$ , indicating that the bond order here is only  $1/2$ , a consequence of the high spin state. This intermediate readily dissociates to  $\text{ThOH}^+$  (<sup>3</sup>Δ) +  $\text{H}$  (<sup>2</sup>S) with the addition of only  $0.06 \text{ eV}$ . Overall, this reaction is calculated to be exothermic by  $0.89 \text{ eV}$ . Once past the first intermediate, exploratory calculations indicate that the quartet surface is significantly higher in energy than the doublet surface (by  $2.8\text{--}4.5 \text{ eV}$ ). Further, because the H atom is lost so easily from **42**, channels like **4TS2/3** and **4TS2/4** cannot plausibly occur. Thus, it is unlikely that the quartet surface plays a significant role in the overall reaction at thermal energies except in the entrance channel.

**Comparison to Experimental Behavior** The PESs of Fig. 4 now permit an analysis of the experimental observations in

Fig. 1. Clearly, the exothermic formation of  $\text{ThO}^+ + \text{D}_2$  and  $\text{DThO}^+ + \text{D}$  can be explained by evolution along the doublet surface leading to the common intermediate  ${}^2\mathbf{2}$ ,  $\text{DThOD}^+$ . At low kinetic energies, products are formed by passing over  ${}^2\text{TS2/3}$  and  ${}^2\text{TS2/4}$ , respectively. Competition between these two channels is explored more thoroughly in the next section. As the energy is increased, a new channel for reaction 6 becomes available, leading to a small increase in the  $[\text{Th},\text{O},\text{D}]^+$  cross-section. According to the PES shown in Fig. 4, this new channel could be associated with evolution along the quartet surface over  ${}^4\text{TS1/2}$ , leading to formation of  $\text{ThOD}^+ ({}^3\Delta) + \text{D}$ . Although calculations indicate that  ${}^4\text{TS1/2}$  lies 0.1–1.4 eV below the reactants, this entropically disfavored tight TS could lead to the appearance of an “endothermic” feature in the cross-sections, as discussed further below. Other possibilities include formation of excited states of either  $\text{HThO}^+$  or  $\text{ThOH}^+$  (as listed in Tables S1 and S2) although these were not explored fully.

Starting at about 1 eV, both the  $\text{DThO}^+$  and  $\text{ThOD}^+$  products can begin to dissociate by losing a D atom to form  $\text{ThO}^+$ , resulting in the increase observed in the  $\text{ThO}^+$  cross-section and concomitant decrease in the  $\text{DThO}^+$  cross-section. This conversion is also evident in the branching ratio starting at 1 eV, Fig. 2. At still higher energies, above  $\text{D}_0(\text{O}-\text{D}_2)$  and  $\text{D}_0(\text{DO}-\text{D})$ , both the  $\text{ThO}^+$  and  $\text{DThO}^+$  cross-sections decrease even more rapidly as these products can dissociate to form  $\text{Th}^+ + \text{O}$  and  $\text{Th}^+ + \text{OD}$ , respectively.

### Theoretical Branching Ratios

Having characterized the potential energy surface for the competing reactions 5–7, it is now possible to model the experimental  $\text{ThO}^+/\text{HThO}^+$  branching ratio. Previously, Zhou and Schlegel [28] calculated the  $\text{ThO}^+/\text{HThO}^+$  branching ratio using RRKM theory and energies and molecular parameters calculated at various levels of theory. Despite  $\text{ThO}^+$  being more thermodynamically favorable, RRKM calculations favor  $\text{HThO}^+$  heavily, with a branching ratio of 11:89, in strong disagreement with the experimentally observed ratio of  $\text{ThO}^+/\text{HThO}^+ = 65:35$  [9, 16]. While somewhat surprising, the result can be understood because RRKM favors reactions where the transition state has low frequencies compared to transition states with higher frequencies. As pointed out previously by Zhou and Schlegel,  ${}^2\text{TS2/4}$  is

much “looser” than the corresponding  ${}^2\text{TS2/3}$  as observed by the vibrational frequencies of these TSs in Table 3. Figure 5 shows that this is a result of the constrained geometry of  ${}^2\text{TS2/3}$  compared to the much more open structure of  ${}^2\text{TS2/4}$ .

Here, we calculate branching ratios according to RRKM and PST rate constants using energies calculated at multiple levels of theory. The results presented in Table 4 assume that  ${}^2\text{TS2/3}$  and  ${}^2\text{TS2/4}$  represent the rate-determining step (rds) to reactions 5 and 6 from  ${}^2\mathbf{2}$ , respectively. Energies available for reaction are taken from the energies of these transition states relative to the reactant asymptote before and after spin-orbit corrections. Molecular parameters used for  ${}^2\mathbf{2}$ ,  ${}^2\text{TS2/3}$ , and  ${}^2\text{TS2/4}$  were taken from the structures optimized at the B3LYP/SDD/6–311++G(3df,3p) level of theory for the smaller basis sets (SDD and Seg. SDD) and the PBE0/cc-pVQZ/cc-pVTZ level of theory for the correlation consistent basis sets. These frequencies are listed in Table 3.

Table 4 shows that RRKM  $\text{ThO}^+/\text{HThO}^+$  branching ratios predict that the  $\text{HThO}^+$  product is favored in every case for energies uncorrected for spin-orbit interactions. Correcting for spin-orbit energies moves the predictions closer to experiment but still favors the  $\text{HThO}^+$  product in every case except CCSD(T)/SDD. These RRKM results are similar to those of Zhou and Schlegel, 11:89 [28]. Zhou and Schlegel explained this discrepancy as likely being a result of the large energies involved so that the competition was no longer statistical [28].

Zhou and Schlegel [28] overcame this limitation by exploring a semi-classical trajectory simulation that found a branching ratio of  $\text{ThO}^+/\text{HThO}^+ \sim 80:20$ , much closer to experiment, but still not quantitative. We believe that the main weakness in the RRKM analysis is that it begins at  ${}^2\mathbf{2}$  so that no history of the reactants is considered. In reality, angular momentum constraints limit the number of successful trajectories for the protiated and deuterated versions of both reactions 5 and 6. More specifically, the reduced mass ( $\mu$ ) of the  $\text{ThO}^+ + \text{H}_2$  products is 1.999 amu, whereas the  $\text{HThO}^+ + \text{H}$  products are half that, 1.004 amu. In both cases, the reduced mass of the products is much smaller than that of the reactants,  $\mu = 16.713$  amu, such that both channels can only conserve angular momentum for smaller impact parameters. (Similar relationships constrain reactions 5 and 6, where the reduced masses are 3.96, 1.99, and 18.41 amu, respectively.) This tendency is overcome to some extent by the large exothermicity of both

**Table 3.** Frequencies ( $\text{cm}^{-1}$ ) of  ${}^2\mathbf{2}$ ,  ${}^2\text{TS2/3}$ , and  ${}^2\text{TS2/4}$  from structures optimized using the indicated level of theory (frequencies scaled by 0.989)

${}^2\mathbf{2}$		${}^2\text{TS2/3}$		${}^2\text{TS2/4}$	
B3LYP <sup>a</sup>	PBE0 <sup>b</sup>	B3LYP <sup>a</sup>	PBE0 <sup>b</sup>	B3LYP <sup>a</sup>	PBE0 <sup>b</sup>
330	326	1519i	1398i	1651i	2099i
416	467	815	851	221	239
425	473	1023	1065	276	297
700	726	1192	1201	330	299
1627	1641	1531	1567	820	851
3777	3803	1865	1892	1574	1588

<sup>a</sup>Structures optimized using B3LYP/SDD/6–311++G(3df,3p)

<sup>b</sup>Structures optimized using PBE0/cc-pVQZ/cc-pVTZ

**Table 4.** Branching ratios ( $\text{ThO}^+/\text{HThO}^+$ ) at 0 eV/K calculated using Rice–Ramsperger–Kassel–Marcus (RRKM) and phase space theory (PST) with energies calculated at several levels of theory<sup>a</sup>

Method		SDD <sup>b</sup>	Seg. SDD <sup>c</sup>	cc-pwCVQZ <sup>d</sup>	CBS <sup>e</sup>
CCSD(T) <sup>f</sup>	RRKM	<b>57:43</b> (31:69)	23:77 (14:86)	21:79 (13:87)	22:78 (14:86)
	PST	94:6 (87:13)	83:17 ( <b>75:25</b> )	82:18 ( <b>75:25</b> )	83:17 (76:24)
B3LYP	RRKM	14:86 (9:91)	12:88 (8:92)	12:88 (8:92)	11:89 (8:92)
	PST	<b>75:25 (68:32)</b>	<b>71:29 (65:35)</b>	<b>72:28 (65:35)</b>	<b>72:28 (66:34)</b>
B3PW91	RRKM	14:86 (9:91)	11:89 (8:92)	12:88 (8:92)	12:88 (8:92)
	PST	<b>75:25 (68:32)</b>	<b>72:28 (65:35)</b>	<b>74:26 (67:33)</b>	<b>73:27 (67:33)</b>
BHLYP	RRKM	42:58:(22:78)	30:70 (17:83)	34:66 (18:82)	32:68 (18:82)
	PST	91:9 (82:18)	86:14 (78:22)	88:12 (80:20)	88:12 (80:20)
M06	RRKM	14:86 (9:91)	12:88 (7:93)	11:89 (7:93)	12:88 (8:92)
	PST	<b>74:26 (67:33)</b>	<b>69:31 (63:37)</b>	<b>71:29 (65:35)</b>	<b>73:27 (66:34)</b>
PBE0	RRKM	15:85 (10:90)	12:88 (9:91)	13:87 (9:91)	12:87 (9:91)
	PST	76:24 ( <b>69:31</b> )	<b>73:27 (67:33)</b>	<b>75:25 (69:31)</b>	<b>75:25 (68:32)</b>

<sup>a</sup>Energies used in calculating branching ratios are taken from Table 2 or Table S4 in Supplementary Material after (before) correcting for spin-orbit energy. Values in bold are within 10% of the experimental ratio of 65:35 at thermal energies

<sup>b</sup>Method/SDD/6–311++G(3df,3p)/B3LYP/SDD/6–311++G(3df,3p)

<sup>c</sup>Method/Seg. SDD/6–311++G(3df,3p)/B3LYP/SDD/6–311++G(3df,3p)

<sup>d</sup>Method/cc-pwCVQZ/6–311++G(3df,3p)/PBE0/cc-pVQZ/cc-pVTZ

<sup>e</sup>Complete basis set extrapolation using Eqs. 3 and 4, Method/cc-pwCVXZ/cc-pwCVXZ/PBE0/cc-pVQZ/cc-pVTZ where X = T, Q

<sup>f</sup>Molecular constants used in these calculations are taken from B3LYP/SDD/(6–311++G(3df,3p)). For SDD and Seg. SDD calculations and PBE0/cc-pVQZ/cc-pVTZ for cc-pwCVQZ and CBS calculations, see Table 3

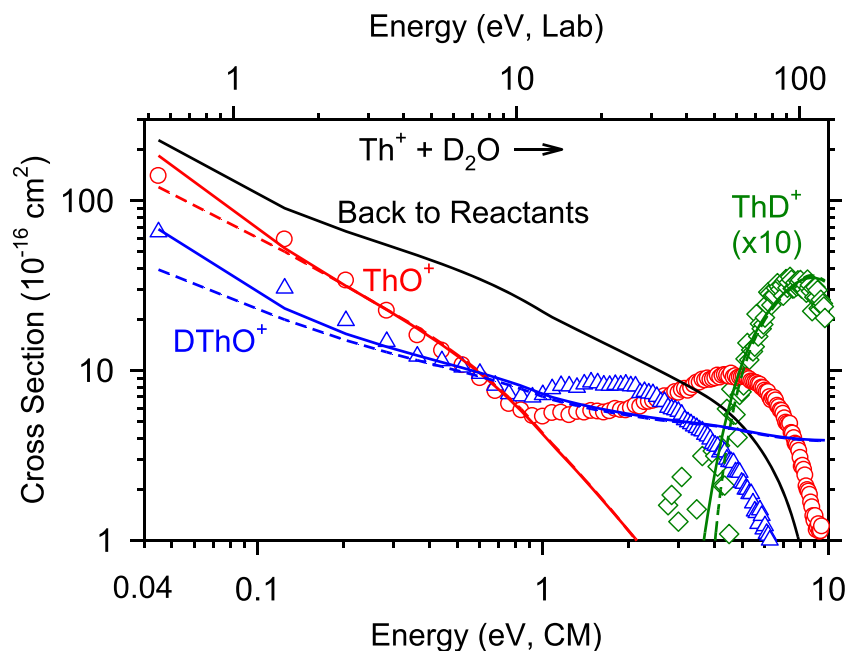
channels (even considering their rds transition states). Nevertheless, angular momentum conservation clearly favors reaction 5 and its protiated variant, in agreement with the observed behavior. Although the reduced mass argument is only semi-quantitative in nature, it definitely indicates that properly accounting for angular momentum conservation is needed to correctly predict the branching ratio.

Here, we account for this quantitatively by utilizing PST, which explicitly requires conservation of angular momentum from the reactants. Unlike the RRKM calculations, the PST branching ratios heavily favor  $\text{ThO}^+$  before correcting for spin-orbit effects. Accounting for spin-orbit energy, the PST branching ratios shift more in favor of  $\text{ThO}^+$ . Now, accurately predicting the experimental branching ratio depends on the details of the energies used for the two competing transition states. PST branching ratios calculated from B3LYP, B3PW91, M06, and PBE0 energies (with all basis sets) are all within  $\pm 11\%$  of the observed experimental branching ratio of 65/35. These ratios result from available energies of 2.48–2.97 eV for  ${}^2\text{TS2/3}$  and 1.29–1.70 eV for  ${}^2\text{TS2/4}$  after including spin-orbit effects, Tables 2 and S4, with  $E_{\text{TS2/4}} - E_{\text{TS2/3}} = 1.08$ –1.29. By contrast, both CCSD(T) and BHLYP calculations are skewed heavily toward formation of  $\text{ThO}^+$ . Here, the CCSD(T) calculations yield energies of 2.15–2.75 eV for  ${}^2\text{TS2/3}$  and 0.72–1.33 eV for  ${}^2\text{TS2/4}$  with  $E_{\text{TS2/4}} - E_{\text{TS2/3}} = 1.31$ –1.43. This suggests that an energy difference between the transition states towards the lower end of  $\sim 1.1$  eV is needed to correctly predict the observed branching ratio.

### Phase Space Theory Modeling of Cross-Sections

A much more stringent test of the theory is to model the kinetic energy dependence of reactions 5 and 6. Clearly, PST is needed and we considered two approaches, both of which use the trajectory model for the total collision probability. These models ignore

any potential spin changes in the reaction; however, the mixed spin nature of the  $\text{Th}^+ J = 3/2$  ground level argues that any effects resulting from a change in spin should be minimal. In the first approach, each channel is modeled as above, using the rds for the competing reactions (i.e.,  ${}^2\text{TS2/3}$  and  ${}^2\text{TS2/4}$ , respectively). This approach is justifiable because reactions 5 and 6 pass through a common intermediate,  ${}^2\mathbf{2}$ , so that the only difference in reaction rates of each channel comes from their rds. Here, molecular parameters (vibrational frequencies and rotational constants) taken from B3LYP/SDD/6–311++G(3df, 3p) optimized structures of deuterated  ${}^2\text{TS2/3}$  and  ${}^2\text{TS2/4}$  are used in the modeling. These PST model cross-sections can be found in Fig. 6 and Fig. 2 shows the prediction of the branching ratios. In both cases, the PST model replicates the experimental results well at low energies for reactions 5 and 6 and the threshold region for reaction 7, discussed further below. Above 1 eV, the PST model fails primarily because these calculations do not account for the decomposition of  $\text{DThO}^+$  into  $\text{ThO}^+ + \text{D}$ , starting at  $1.10 \pm 0.14$  eV. This is particularly evident in Fig. 2. In addition, the minor contribution from the additional pathway forming  $[\text{Th}, \text{O}, \text{D}]^+$ , postulated to proceed over  ${}^4\text{TS1/2}$  above, is not included in this model. A PST model that did include competition between  ${}^2\text{TS2/3}$ ,  ${}^2\text{TS2/4}$ , and  ${}^4\text{TS1/2}$  was attempted and demonstrates that apparent “endothermic behavior” as observed experimentally can occur for the  ${}^4\text{TS1/2}$  channel even with its energy as much as 0.5 eV below reactants, comparable to the calculations (Table 2). This model is not quantitative, however, requiring significant scaling of this channel to reproduce the data, which then interferes with the low energy behavior of the two major channels. Given the loosely bound nature of the D atom to  $\text{ThOD}^+$  along the quartet surface, this scaling could easily be a consequence of inaccurate vibrational frequencies associated with this weak interaction. As such scaling makes this interpretation even more speculative, it was not pursued further.



**Figure 6.** Product cross-sections for the reaction of  $\text{Th}^+$  with  $\text{D}_2\text{O}$  (points) compared to the phase space theory model discussed in the text convoluted over the distributions of internal and translational reactant energies (solid lines) and excluding these distributions (dashed lines). The black line shows the predicted cross-section for returning to reactants

The *only* adjustable parameters for the PST model are the threshold energies for each channel, which correspond to the rds for each process. The models shown in Figs. 2 and 6 utilize thresholds of  $E_0(5) = -2.0 \pm 0.2$  eV and  $E_0(6) = -1.0 \pm 0.1$  eV in order to reproduce the experimental data. Importantly, the energy difference between these two values needs to be 0.9–1.0 eV in order to reproduce experiment. Note that this difference is in agreement with the value of about 1.1 eV obtained above from modeling the thermal branching ratio alone. Further, we can compare these energies with those calculated theoretically for  ${}^2\text{TS2/3}$  and  ${}^2\text{TS2/4}$  in Table 2 (ignoring the small zero-point energy differences). Values for  ${}^2\text{TS2/3}$  range from  $-2.26$  to  $-2.97$  eV,  $0.26$ – $0.97 \pm 0.2$  eV lower than the PST modeling, whereas values for  ${}^2\text{TS2/4}$  lie at  $-0.96$  to  $-1.68$  eV compared to the PST value of  $-1.0 \pm 0.1$  eV. BHLYP values are nearly in agreement with the PST modeling. Theoretical energy differences between the two TSs range from 1.15 to 1.41 eV, slightly larger than the preferred value of  $\sim 1 \pm 0.1$  eV.

The second modeling approach tried assumes that  ${}^2\text{TS1/2}$  is the rds in both reactions 5 and 6. The PST model is adapted to calculate the rate through this “tight” transition state and utilizes the molecular parameters calculated in the B3LYP/SDD/6–311++G(3df, 3p) optimized structure of deuterated  ${}^2\text{TS1/2}$ . Because  ${}^2\text{TS1/2}$  leads to both sets of products from reactions 5 and 6, the total cross-section was modeled and led to an energy for  ${}^2\text{TS1/2}$  of  $-2.0 \pm 0.2$  eV. This value can be compared with the theoretical values in Table 2, which range from  $-0.46$  to  $-1.58$  eV, with the CCSD(T) value at  $-0.68$  eV. The discrepancies of  $1.5$ – $0.4 \pm 0.2$  eV suggest that this is not a useful means of reproducing the data.

Regardless of the approach used to model reactions 5 and 6, the PST model yields  $E_0(7) = 3.55 \pm 0.10$  eV for formation of

$\text{ThD}^+ + \text{OD}$ , similar to the threshold obtained by modeling with Eq. 1, Table 1. This value is much higher than the expected threshold of  $2.73 \pm 0.07$  eV suggested by the  $\text{D}_0(\text{Th}^+-\text{D})$  value determined previously [25]. The discrepancy is probably because the PST model does not account for the decomposition of  $\text{DThO}^+$  into  $\text{ThO}^+ + \text{D}$ , nor for the higher energy pathway forming  $\text{ThOD}^+ + \text{D}$ , such that the competition among reactions 5–7 is not accurately portrayed at energies above about 1 eV.

## Discussion

A major motivation for our recent work with thorium is to provide experimental benchmarks to which theoretical values can be compared. Previous studies of the reactions of thorium with carbon monoxide [26] and hydrogen [25] indicate enthalpies of reaction for the perprotiated analogues of reactions 5 and 7 are  $\Delta_r H(5) = -3.54 \pm 0.14$  eV and  $\Delta_r H(7) = 2.65 \pm 0.07$  eV relative to the reactants, respectively. PST modeling in this work indicates that  ${}^2\text{TS2/3}$  and  ${}^2\text{TS2/4}$  lie  $2.0 \pm 0.2$  and  $1.0 \pm 0.1$  eV below the reactants, respectively. Table 5 compares these experimental values to CCSD(T) calculated values, two other select levels of theory, and values from the literature [28]. Although Zhou and Schlegel reported results from several approaches, they considered the most reliable results to be PW91/ZORA-SO (which includes spin-orbit corrections) and CCSD(T)/SDD+ (a composite approach using a larger basis set). These two approaches give similar energy values except for  ${}^2\text{TS2/3}$  (differing by 0.68 eV), hence, only the CCSD(T)/SDD+ values are listed in Table 5 as these results agree better with the present experiments. Comparison with the present

**Table 5.** Comparison of experimentally derived energies (eV) and branching ratios to theoretically derived values calculated at the indicated level of theory and basis set

	Exp. <sup>a</sup>	CCSD(T) SDD <sup>b</sup>	Seg. SDD <sup>c</sup>	cc-pwCVQZ <sup>d</sup>	CBS <sup>e</sup>	BHLYP CBS <sup>e</sup>	M06 CBS <sup>e</sup>	CCSD(T) SDD <sup>f</sup>
$\Delta_r H(5)$ , $\text{ThO}^+ + \text{H}_2$	-3.54 (0.14) <sup>g</sup>	-3.23	-3.72	-3.77	-3.74	-3.35	-3.78	-3.39
$\Delta_r H(7)$ , $\text{ThH}^+ + \text{OH}$	2.65 (0.07) <sup>h</sup>	1.80	1.65	2.35	2.36	2.00	2.41	
<sup>2</sup> TS2/3	-2.0 (0.2) <sup>i</sup>	-2.15	-2.50	-2.73	-2.70	-2.26	-2.67	-2.20
<sup>2</sup> TS2/4	-1.0 (0.1) <sup>i</sup>	-0.72	-1.19	-1.33	-1.29	-0.96	-1.52	-1.56
MAD <sup>j</sup>		0.40 (0.31)	0.47 (0.39)	0.40 (0.23)	0.37 (0.22)	0.29 (0.26)	0.42 (0.21)	0.30 (0.22)
$\text{ThO}^+/\text{HTHo}^+$ <sup>k</sup>	65:35	94:6	83:17	82:18	83:17	88:12	73:27	~80:20
Deviation <sup>l</sup>		±29	±18	±18	±18	±23	±8	±15

<sup>a</sup>Experimental values with uncertainties in parentheses. <sup>b</sup>CCSD(T)/SDD/6-311++G(3df,3p)//B3LYP/SDD/6-311++G(3df,3p). <sup>c</sup>CCSD(T)/Seg. SDD/6-311++G(3df,3p)//B3LYP/SDD/6-311++G(3df,3p). <sup>d</sup>CCSD(T)/cc-pwCVQZ/6-311++G(3df,3p)//PBE0/cc-pVQZ/cc-pVTZ. <sup>e</sup>Complete basis set extrapolation using Eqs. 3 and 4, Method/cc-pVXZ/cc-pVXZ//PBE0/cc-pVQZ/cc-pVTZ where X = T, Q. <sup>f</sup>Results from Ref. [28] assuming intermediate <sup>2</sup>1 lies 0.87 eV below ground state reactants. Energies are similar to the B3LYP/SDD results of Ref. [27]. Here, the branching ratio is derived from trajectory results, see text. <sup>g</sup>Calculated using  $D_0(\text{Th}^+-\text{O}) = 8.57 \pm 0.14$  eV from Ref. [26] and  $D_0(\text{O}-\text{H}_2) = 5.0348$  eV from Ref. [84]. <sup>h</sup>Calculated using  $D_0(\text{Th}^+-\text{H}) = 2.45 \pm 0.07$  eV from Ref. [25] and  $D_0(\text{HO}-\text{H}) = 5.101$  eV from Ref. [84]. <sup>i</sup>PST fit of reactions 5 and 6. See Figs. 2 and 6 and text. <sup>j</sup>Mean absolute deviation (1 standard deviation). <sup>k</sup>Experimental branching ratio from Refs. [9, 16]. Theoretical branching ratios are calculated using the indicated method and basis set with PST after correcting for spin-orbit energies. See text and Table 4. <sup>l</sup>Deviation of theoretical branching ratio from the experimentally observed ratio

calculations is hindered by the fact that Zhou and Schlegel do not report an energy for the  $\text{Th}^+ + \text{H}_2\text{O}$  reactants, but rather refer to the results of Mazzone et al. [27] citing a relative energy for <sup>2</sup>1 of -0.87 eV.

A couple of trends can be observed from Table 5. The reaction forming the  $\text{ThO}^+ + \text{H}_2$  products, the analogue of reaction 5, has an exothermicity that is reasonably well predicted by theory, with deviations between -0.24 and +0.31 eV. In contrast, the endothermicity in the formation of  $\text{ThH}^+ + \text{OH}$  in the analogue of reaction 7 is systematically too low, by 0.2–0.9 eV. This latter deviation agrees with the more extensive theoretical exploration in our study of the  $\text{Th}^+ + \text{H}_2/\text{D}_2$  reactions [25]. Likewise, all calculations predict that <sup>2</sup>TS2/3 is lower than found by the PST modeling, although CCSD(T)/SDD and CCSD(T)/SDD+ results are within and BHLYP/CBS results are just outside the experimental uncertainty. For <sup>2</sup>TS2/4, the CCSD(T)/SDD and BHLYP/CBS approaches predict a higher energy than the PST model result (with the BHLYP/CBS value within experimental uncertainty, which is why this result is singled out here), whereas all other approaches listed predict lower energies (by 0.2–0.6 eV), with the CCSD(T)/SDD+ results showing the largest deviation.

The mean absolute deviations (MADs) listed in Table 5 between these four experimental energies and theoretical values indicate similar abilities to reproduce the experimental values, with BHLYP/CBS and CCSD(T)/SDD+ (which is favored because it does not include the problematic comparison with  $\Delta_r H(7)$ ) being slightly better and CCSD(T)/Seg. SDD slightly worse than the other approaches. Although CCSD(T)/SDD and BHLYP/CBS have two values above and two values below experiment, all other levels of theory are systematically low. It should be realized that without the spin-orbit corrections (included in all the present theoretical values in Table 5), the results would be considerably worse for all levels of theory. Such deviations for actinide thermochemistry are not unprecedented with most levels of theory systematically overestimating bond energies for  $\text{ThH}^+$  (by 0.0–0.5 eV),  $\text{ThC}^+$  (by 0.0–0.6 eV), and  $\text{ThO}^+$  (by 0.0–0.4 eV) (which leads

to low values on the PES for these two asymptotes) [25, 26]. In these works, more advanced theoretical approaches [85, 86] provided more accurate results, but are beyond the scope of an entire PES.

In analyzing the performance of theory, it is also instructive to examine the predicted branching ratio at thermal energies calculated using PST and the energies of <sup>2</sup>TS2/3 and <sup>2</sup>TS2/4 for each level of theory. This comparison is also listed in Table 5. Such an analysis indicates that although the CCSD(T)/SDD calculations yield comparable results to the correlation consistent basis sets for the thermochemical values, it deviates by ±29% from the experimental branching ratio compared to ±18% for the CCSD(T) using correlation consistent basis sets and ±23% for BHLYP/CBS. M06/CBS gives the best result with a deviation of only ±8% (and the reason this particular level of theory is included in this comparison). Note that this level has the smallest difference in energies between <sup>2</sup>TS2/3 and <sup>2</sup>TS2/4, 1.15 eV and similar to the experimental value of about  $1.0 \pm 0.1$  eV, compared with 1.30–1.43 eV for the other methods in Table 5. Consistent with these observations is the fact that for the trajectory results of Zhou and Schlegel [28], the energies used were those calculated at the PW91/SDD level where the energy difference between <sup>2</sup>TS2/3 and <sup>2</sup>TS2/4 was 1.18 eV. Although the resulting ~80:20 branching ratio is in reasonable agreement with experiment, the result was obtained with only 16 trajectories that were initiated from <sup>2</sup>TS1/2. Thus, the return to reactants, which limits the overall efficiency of the reaction and also competes with reactions 5 and 6, was not considered nor was the distribution of angular momentum available to the species likely to be accurate.

It is important to also realize that these theoretical branching ratios represent relative rates rather than absolute rates, so that a particular method can reproduce the experimental branching ratio while simultaneously incorrectly predicting the absolute rates. Therefore, a comparison of theoretical branching ratios to the experimentally observed ratios may be a valuable metric to evaluate theoretical methods and basis sets; however, without absolute rates they may be misleading. Further, the snapshot of

predicting only the thermal branching ratio is clearly not as demanding as reproducing the interesting kinetic energy dependence over an extended range, such as that shown in Figs. 2 and 6.

## Acknowledgements

This work is supported by the Heavy Element Chemistry Program, Office of Basic Energy Sciences, U. S. Department of Energy, through Grant No. DE-SC0012249 (PBA). We also thank the Center for High Performance Computing at the University of Utah for the generous allocation of computer time.

## References

- Armentrout, P.B., Hodges, R.V., Beauchamp, J.L.: Endothermic reactions of uranium ions with  $N_2$ ,  $D_2$  and  $CD_4$ . *J. Chem. Phys.* **66**, 4683–4688 (1977)
- Armentrout, P.B., Hodges, R.V., Beauchamp, J.L.: Metal atoms as super bases: the gas phase proton affinity of uranium. *J. Am. Chem. Soc.* **99**, 3162–3263 (1977)
- Armentrout, P.B., Beauchamp, J.L.: Collision induced dissociation of  $UO^+$  and  $UO_2^+$ . *Chem Phys.* **50**, 21–25 (1980)
- Armentrout, P.B., Beauchamp, J.L.: Reactions of  $U^+$  and  $UO^+$  with  $O_2$ ,  $CO$ ,  $CO_2$ ,  $COS$ ,  $CS_2$  and  $D_2O$ . *Chem. Phys.* **50**, 27–36 (1980)
- Armentrout, P.B., Beauchamp, J.L.: Thermochemistry of uranium halide ions. Reactions of  $U^+$  with  $CH_3F$ ,  $SiF_4$ ,  $CH_3Cl$ , and  $CCl_4$ . *J. Phys. Chem.* **85**, 4103–4105 (1981)
- Heinemann, C., Schwarz, H.:  $NUO^+$ , a new species isoelectronic to the uranyl dication  $UO$ . *Chem. Eur. J.* **1**, 7–11 (1995)
- Cornehl, H.H., Heinemann, C., Marçalo, J., de Matos, A.P., Schwarz, H.: The “bare” uranyl(2+) ion,  $UO_2^{2+}$ . *Ang. Chem. Int. Ed.* **35**, 891–894 (1996)
- Heinemann, C., Cornehl, H.H., Schwarz, H.: Hydrocarbon activation by “bare” uranium cations: formation of a cationic uranium–benzene complex from three ethylene units. *J. Organomet. Chem.* **501**, 201–209 (1995)
- Cornehl, H.H., Wesendrup, R., Diefenbach, M., Schwarz, H.: A comparative study of oxo-ligand effects in the gas-phase chemistry of atomic lanthanide and actinide cations. *Chem. Eur. J.* **3**, 1083–1090 (1997)
- Schröder, D., Diefenbach, M., Klapötke, T.M., Schwarz, H.:  $UF_3^+$ —a thermochemically stable diatomic trication with a covalent bond. *Ang. Chem. Int. Ed.* **38**, 137–140 (1999)
- Gibson, J.K.: Gas-phase transuranium organometallic chemistry: reactions of  $Np^+$ ,  $Pu^+$ ,  $NpO^+$ , and  $PuO^+$  with alkenes. *J. Am. Chem. Soc.* **120**, 2633–2640 (1998)
- Gibson, J.K.: Actinide gas-phase chemistry: reactions of  $An^+$  and  $AnO^+$  [ $An = Th, U, Np, Pu, Am$ ] with nitriles and butylamine. *Inorg. Chem.* **38**, 165–173 (1999)
- Gibson, J.K.: Gas-phase reactions of  $An^+$  and  $AnO^+$  [ $An = Th, U, Np, Pu, Am$ ] with halogenated hydrocarbons [ $C_{14}F_{24}$ ,  $C_3F_6$ ,  $C_2H_4Cl_2$  and  $C_2H_4Br_2$ ]. In *Radiochim. Acta*, 1999; Vol. 84, p 135
- Gibson, J. K., Haire, R. G., Berkelium and californium organometallic ions. In *Radiochim. Acta*, 2001; Vol. 89, p 363
- Gibson, J.K., Haire, R.G.: Gas-phase chemistry of bare and oxo-ligated protactinium ions: a contribution to a systematic understanding of actinide chemistry. *Inorg. Chem.* **41**, 5897–5906 (2002)
- Santos, M., Marçalo, J., Matos, A.P.d., Gibson, J.K., Haire, R.G.: Gas-phase oxidation reactions of neptunium and plutonium ions investigated via Fourier transform ion cyclotron resonance mass spectrometry. *J. Phys. Chem. A.* **106**, 7190–7194 (2002)
- Santos, M., Marçalo, J., Leal, J.P., Matos, A.P.d., Gibson, J.K., Haire, R.G.: FTICR-MS study of the gas-phase thermochemistry of americium oxides. *Int. J. Mass Spectrom.* **228**, 457–465 (2003)
- Goncharov, V., Heaven, M.C.: Spectroscopy of the ground and low-lying excited states of  $ThO^+$ . *J. Chem. Phys.* **124**, 064312 (2006)
- Heaven, M.C.: Probing actinide electronic structure using fluorescence and multi-photon ionization spectroscopy. *Phys. Chem. Chem. Phys.* **8**, 4497–4509 (2006)
- Gibson, J.K., Haire, R.G., Marçalo, J., Santos, M., Leal, J.P., Pires de Matos, A., Tyagi, R., Mrozik, M.K., Pitzer, R.M., Bursten, B.E.: FTICR/MS studies of gas-phase actinide ion reactions: fundamental chemical and physical properties of atomic and molecular actinide ions and neutrals. *Eur. Phys. J. D.* **45**, 133–138 (2007)
- Marçalo, J., Gibson, J.K.: Gas-phase energetics of actinide oxides: an assessment of neutral and cationic monoxides and dioxides from thorium to curium. *J. Phys. Chem. A.* **113**, 12599–12606 (2009)
- Pereira, C.C.L., Marsden, C.J., Marçalo, J., Gibson, J.K.: Actinide sulfides in the gas phase: experimental and theoretical studies of the thermochemistry of  $An$  ( $An = Ac, Th, Pa, U, Np, Pu, Am$  and  $Cm$ ). *Phys. Chem. Chem. Phys.* **13**, 12940–12958 (2011)
- Heaven, M.C., Barker, B.J., Antonov, I.O.: Spectroscopy and structure of the simplest actinide bonds. *J. Phys. Chem. A.* **118**, 10867–10881 (2014)
- Cox, R.M., Armentrout, P.B., de Jong, W.A.: Activation of  $CH_4$  by  $Th^+$  as studied by guided ion beam mass spectrometry and quantum chemistry. *Inorg. Chem.* **54**, 3584–3599 (2015)
- Cox, R.M., Armentrout, P.B., de Jong, W.A.: Reactions of  $Th^+ + H_2$ ,  $D_2$ , and  $HD$  studied by guided ion beam tandem mass spectrometry and quantum chemical calculations. *J. Phys. Chem. B.* **120**, 1601–1614 (2016)
- Cox, R.M., Citir, M., Armentrout, P.B., Battey, S.R., Peterson, K.A.: Bond energies of  $ThO^+$  and  $ThC^+$ : a guided ion beam and quantum chemical investigation of the reactions of thorium cation with  $O_2$  and  $CO$ . *J. Chem. Phys.* **144**, 184309 (2016)
- Mazzone, G., Michelini, M.d.C., Russo, N., Sicilia, E.: Mechanistic aspects of the reaction of  $Th^+$  and  $Th^{2+}$  with water in the gas phase. *Inorg. Chem.* **47**, 2083–2088 (2008)
- Zhou, J., Schlegel, H.B.: Ab initio molecular dynamics study of the reaction between  $Th^+$  and  $H_2O$ . *J. Phys. Chem. A.* **114**, 8613–8617 (2010)
- Gilbert, R.G., Smith, S.C.: Theory of unimolecular and recombination reactions. Blackwell Scientific, London (1990)
- Robinson, P.J., Holbrook, K.A.: Unimolecular reactions. Wiley Interscience, New York (1972)
- Loh, S.K., Hales, D.A., Lian, L., Armentrout, P.B.: Collision-induced dissociation of  $Fe_n^+$  ( $n = 2-10$ ) with Xe: ionic and neutral iron cluster binding energies. *J. Chem. Phys.* **90**, 5466–5485 (1989)
- Schultz, R.H., Armentrout, P.B.: Reactions of  $N_4^+$  with rare gases from thermal to 10 eV c.m.: collision-induced dissociation, charge transfer, and ligand exchange. *Int. J. Mass Spectrom. Ion Process.* **107**, 29–48 (1991)
- Haynes, C.L., Armentrout, P.B.: Thermochemistry and structures of  $CoC_3H_6^+$ : metallacycle and metal-alkene isomers. *Organomet.* **13**, 3480–3490 (1994)
- Clemmer, D.E., Chen, Y.-M., Khan, F.A., Armentrout, P.B.: State-specific reactions of  $Fe^+(a^6D, a^6F)$  with  $D_2O$  and reactions of  $FeO^+$  with  $D_2$ . *J. Phys. Chem.* **98**, 6522–6529 (1994)
- Kickel, B.L., Armentrout, P.B.: Reactions of  $Fe^+$ ,  $Co^+$  and  $Ni^+$  with silane. Electronic state effects and  $M^+-SiH_x$  ( $x = 0-3$ ) bond energies. *J. Am. Chem. Soc.* **117**, 764–773 (1995)
- Kickel, B.L., Armentrout, P.B.: Guided ion beam studies of the reactions of group 3 metal ions ( $Sc^+$ ,  $Y^+$ ,  $La^+$ , and  $Lu^+$ ) with silane. Electronic state effects, comparison to reactions with methane, and  $M^+-SiH_x$  ( $x = 0-3$ ) bond energies. *J. Am. Chem. Soc.* **117**, 4057–4070 (1995)
- Sievers, M.R., Chen, Y.-M., Elkind, J.L., Armentrout, P.B.: Reactions of  $Y^+$ ,  $Zr^+$ ,  $Nb^+$ , and  $Mo^+$  with  $H_2$ ,  $HD$ , and  $D_2$ . *J. Phys. Chem.* **100**, 54–62 (1996)
- Teloy, E., Gerlich, D.: Integral cross sections for ion-molecule reactions. I. The guided beam technique. *Chem. Phys.* **4**, 417–427 (1974)
- Armentrout, P.B.: The kinetic energy dependence of ion-molecule reactions: guided ion beams and threshold measurements. *Int. J. Mass Spectrom.* **200**, 219–241 (2000)
- Ervin, K.M., Armentrout, P.B.: Translational energy dependence of  $Ar^+ + XY \rightarrow ArX^+ + Y$  ( $XY = H_2, D_2, HD$ ) from thermal to 30 eV c.m. *J. Chem. Phys.* **83**, 166–189 (1985)
- Chantry, P.J.: Doppler broadening in beam experiments. *J. Chem. Phys.* **55**, 2746–2759 (1971)
- Light, J.C.: Phase-space theory of chemical kinetics. *J. Chem. Phys.* **40**, 3221–3229 (1964)
- Pechukas, P., Light, J.C.: On detailed balancing and statistical theories of chemical kinetics. *J. Chem. Phys.* **42**, 3281–3291 (1965)

44. Nikitin, E.E.: Statistical theory of exothermic ion-molecule reactions. *Teor. Eksp. Khim.* **1**, 428–435 (1965)
45. Chesnavich, W.J., Bowers, M.T.: Threshold behavior of endoergic bimolecular reactions: a statistical phase space approach. *J. Phys. Chem.* **68**, 901–910 (1978)
46. Langevin, P.: Une formule fondamentale de theorie cinetique. *Ann. Chim. Phys. Ser.* **8**(5), 245–288 (1905)
47. Gioumousis, G., Stevenson, D.P.: Reactions of gaseous molecule ions with gaseous molecules. V. Theory. *J. Chem. Phys.* **29**, 294–299 (1958)
48. Su, T., Bowers, M.T.: Classical ion-molecule collision theory. In: Bowers, M.T. (ed.) *Gas phase ion chemistry*, vol. 1, pp. 83–118. Academic, New York (1979)
49. Su, T., Chesnavich, W.J.: Parameterization of the ion-polar molecule collision rate constant by trajectory calculations. *J. Chem. Phys.* **76**, 5183–5185 (1982)
50. Weber, M.E., Dalleska, N.F., Tjelta, B.L., Fisher, E.R., Armentrout, P.B.: Reaction of  $O_2^+(X^2\Pi_g)$  with  $H_2$ ,  $D_2$ , and HD: guided ion beam studies, mo correlations, and statistical theory calculations. *J. Chem. Phys.* **98**, 7855–7867 (1993)
51. Chesnavich, W.J., Bowers, M.T.: Theory of translationally driven reactions. *J. Phys. Chem.* **83**, 900–905 (1979)
52. Muntean, F., Armentrout, P.B.: Guided ion beam study of collision-induced dissociation dynamics: integral and differential cross sections. *J. Chem. Phys.* **115**, 1213–1228 (2001)
53. Aristov, N., Armentrout, P.B.: Reaction mechanisms and thermochemistry of  $V^+ + C_2H_2p$  ( $p = 1, 2, 3$ ). *J. Am. Chem. Soc.* **108**, 1806–1819 (1986)
54. Weber, M.E., Elkind, J.L., Armentrout, P.B.: Kinetic energy dependence of  $Al^+ + O_2 \rightarrow AlO^+ + O$ . *J. Chem. Phys.* **84**, 1521–1529 (1986)
55. Frisch, M. J., Trucks, G. W., Schlegel, H. B., Scuseria, G. E., Robb, M. A., Cheeseman, J. R., Scalmani, G., Barone, V., Mennucci, B., Petersson, G. A., Nakatsuji, H., Caricato, M., Li, X., Hratchian, H. P., Izmaylov, A. F., Bloino, J., Zheng, G., Sonnenberg, J. L., Hada, M., Ehara, M., Toyota, K., Fukuda, R., Hasegawa, J., Ishida, M., Nakajima, T., Honda, Y., Kitao, O., Nakai, H., Vreven, T., Montgomery Jr., J. A., Peralta, J. E., Ogliaro, F., Bearpark, M. J., Heyd, J., Brothers, E. N., Kudin, K. N., Staroverov, V. N., Kobayashi, R., Normand, J., Raghavachari, K., Rendell, A. P., Burant, J. C., Iyengar, S. S., Tomasi, J., Cossi, M., Rega, N., Millam, N. J., Klene, M., Knox, J. E., Cross, J. B., Bakken, V., Adamo, C., Jaramillo, J., Gomperts, R., Stratmann, R. E., Yazyev, O., Austin, A. J., Cammi, R., Pomelli, C., Ochterski, J. W., Martin, R. L., Morokuma, K., Zakrzewski, V. G., Voth, G. A., Salvador, P., Dannenberg, J. J., Dapprich, S., Daniels, A. D., Farkas, Ö., Foresman, J. B., Ortiz, J. V., Cioslowski, J., Fox, D. J.: *Gaussian 09, revision 01*. Gaussian, Inc.: Wallingford, CT, USA, 2009
56. Peterson, K. A.: Correlation consistent basis sets for actinides. I. The Th and U atoms. *J. Chem. Phys.* **142**, 074105 (2015)
57. Weigand, A., Cao, X., Hangele, T., Dolg, M.: Relativistic small-core pseudopotentials for actinium, thorium, and protactinium. *J. Phys. Chem. A.* **118**, 2519–2530 (2014)
58. Woon, D.E., Dunning Jr., T.H.: Gaussian basis sets for use in correlated molecular calculations. V. Core-valence basis sets for boron through neon. *J. Chem. Phys.* **103**, 4572–4585 (1995)
59. Dunning, T.H.: Gaussian basis sets for use in correlated molecular calculations. I. The atoms boron through neon and hydrogen. *J. Chem. Phys.* **90**, 1007–1023 (1989)
60. Karton, A., Martin, J.M.L.: Comment on: “Estimating the Hartree–Fock limit from finite basis set calculations” [Jensen F (2005) *Theor Chem Acc* 113:267]. *Theor. Chem. Acc.* **115**, 330–333 (2006)
61. Martin, J.M.L.: Ab initio total atomization energies of small molecules—towards the basis set limit. *Chem. Phys. Lett.* **259**, 669–678 (1996)
62. Küchle, W., Dolg, M., Stoll, H., Preuss, H.: Energy-adjusted pseudopotentials for the actinides. Parameter sets and test calculations for thorium and thorium monoxide. *J. Chem. Phys.* **100**, 7535–7542 (1994)
63. Cao, X., Dolg, M., Stoll, H.: Valence basis sets for relativistic energy-consistent small-core actinide pseudopotentials. *J. Chem. Phys.* **118**, 487–496 (2003)
64. Krishnan, R., Binkley, J.S., Seeger, R., Pople, J.A.: Self-consistent molecular orbital methods. XX. A basis set for correlated wave functions. *J. Chem. Phys.* **72**, 650–654 (1980)
65. Lee, C., Yang, W., Parr, R.G.: Development of the Colle–Salvetti correlation-energy formula into a functional of the electron density. *Phys. Rev. B.* **37**, 785–789 (1988)
66. Becke, A.D.: Density-functional thermochemistry. III. The role of exact exchange. *J. Chem. Phys.* **98**, 5648–5652 (1993)
67. Perdew, J.P., Burke, K., Wang, Y.: Generalized gradient approximation for the exchange-correlation hole of a many-electron system. *Phys. Rev. B.* **54**, 16533–16539 (1996)
68. Zhao, Y., Truhlar, D.G.: The M06 suite of density functionals for main group thermochemistry, thermochemical kinetics, noncovalent interactions, excited states, and transition elements: two new functionals and systematic testing of four M06-class functionals and 12 other functionals. *Theor. Chem. Accounts.* **120**, 215–241 (2008)
69. Adamo, C., Barone, V.: Toward reliable density functional methods without adjustable parameters: the PBE0 model. *J. Chem. Phys.* **110**, 6158–6170 (1999)
70. Purvis, G.D., Bartlett, R.J.: A full coupled-cluster singles and doubles model: the inclusion of disconnected triples. *J. Chem. Phys.* **76**, 1910–1918 (1982)
71. Pople, J.A., Head-Gordon, M., Raghavachari, K.: Quadratic configuration interaction. A general technique for determining electron correlation energies. *J. Chem. Phys.* **87**, 5968–5975 (1987)
72. Scuseria, G.E., Janssen, C.L., Schaefer, H.F.: An efficient reformulation of the closed-shell coupled cluster single and double excitation (CCSD) equations. *J. Chem. Phys.* **89**, 7382–7387 (1988)
73. Foresman, J.B., Frisch, A.E.: *Exploring chemistry with electronic structure methods*, 2nd edn. Gaussian, Inc., Pittsburgh, PA (1996)
74. Kesharwani, M.K., Brauer, B., Martin, J.M.L.: Frequency and zero-point vibrational energy scale factors for double-hybrid density functionals (and other selected methods): can anharmonic force fields be avoided? *J. Phys. Chem. A.* **119**, 1701–1714 (2014)
75. Garcia, M.A., Morse, M.D.: Resonant two-photon ionization spectroscopy of jet-cooled OsN: 520–418 nm. *J. Chem. Phys.* **135**, 114304 (2011)
76. Armentrout, P.B., Parke, L., Hinton, C., Citir, M.: Activation of methane by  $Os^+$ : guided ion beam and theoretical studies. *ChemPlusChem.* **78**, 1157–1173 (2013)
77. Blaise, J., Wyrart, J.-F.: *Energy levels and atomic spectra of actinides*, Paris (1992)
78. Sansonetti, J.E., Martin, W.C.: *Handbook of basic atomic spectroscopic data*. *J. Phys. Chem. Ref. Data.* **34**, 1559–2259 (2005)
79. Beyer, T.S., Swinehart, D.F.: Number of multiply-restricted partitions. *Commun. ACM.* **16**, 379 (1973)
80. Stein, S.E., Rabinovitch, B.S.: Accurate evaluation of internal energy level sums and densities including anharmonic oscillators and hindered rotors. *J. Chem. Phys.* **58**, 2438–2445 (1973)
81. Stein, S.E., Rabinovitch, B.S.: On the use of exact state counting methods in RRKM rate calculations. *Chem. Phys. Lett.* **49**, 183–188 (1977)
82. Johnson III, R. D. NIST computational chemistry comparison and benchmark database. NIST Standard Reference Database Number 101, Release 19, <http://cccbdb.nist.gov/>. Accessed 12 Apr 2018
83. Konings, R.J.M., Benes, O., Kovacs, A., Manara, D., Sedmidubsky, D., Gorokhov, L., Iorish, V.S., Yungman, V., Shenyavskaya, E., Osina, E.: The thermodynamic properties of the f-elements and their compounds. Part 2. The lanthanide and actinide oxides. *J. Phys. Chem. Ref. Data.* **43**, 013101 (2014)
84. Goos, E., Burcat, A., Ruscic, B. *Extended Third Millennium Ideal Gas and Condensed Phase Thermochemical Database for Combustion with Updates from Active Thermochemical Tables; ANL-05/20 and TAE 960 Technion-IIT, Aerospace Engineering, and Argonne National Laboratory, Chemistry Division: 2016.* (accessed August 2017)
85. Feller, D., Peterson, K.A., Dixon, D.A.: A survey of factors contributing to accurate theoretical predictions of atomization energies and molecular structures. *J. Chem. Phys.* **129**, 204105 (2008)
86. Vasiliiu, M., Peterson, K.A., Gibson, J.K., Dixon, D.A.: Reliable potential energy surfaces for the reactions of  $H_2O$  with  $ThO_2$ ,  $PaO_2^+$ ,  $UO_2^{2+}$ , and  $UO_2^+$ . *J. Phys. Chem. A.* **119**, 11422–11431 (2015)